

# **Synthesis and Characterization of Doped and Undoped ZnS Thin Films using Chemical Bath Deposition**



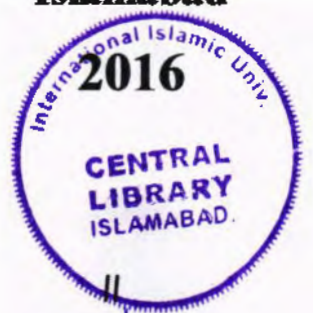
**Student Name: Saima Perveen**

**Registration No: 244-FBAS/MSPHY/S-14**

**Supervisor: Dr. Shaista Shahzada**

**Department of Physics  
Faculty of Basic and Applied Science  
International Islamic University**

**Islamabad**



Accession No. H17283<sup>MM</sup>



MS  
S30  
SAS

X-ray diffraction

Optical properties.

UV-Vis spectrum.

*In the name of Allah, the almighty most*

*Merciful and the most beneficent*



DEPARTMENT OF PHYSICS

FACULTY OF BASIC AND APPLIED SCIENCES

INTERNATIONAL ISLAMIC UNIVERSITY ISLAMABAD

**Synthesis and Characterization of Doped and Undoped ZnS Thin Films  
using Chemical Bath Deposition**

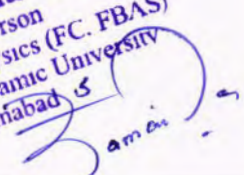
**BY**


**Saima Perveen**

**244-FBAS/MSPHY/S-14**

A thesis submitted to  
**Department of Physics**  
For the award of the degree of  
**MS physics**

**Dr. Shamaila Sajjad**  
Chairperson  
Department of Physics (FC, FBAS)  
International Islamic University  
Islamabad

Signature:   
(Chairperson, Department of physics)

Signature:   
(Dean, FBAS IIU, Islamabad)

**Department of physics International Islamic University  
Islamabad**

Dated: 31-08-2016

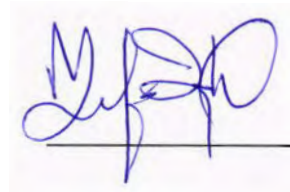
**Final approval**

It is certified that the work presents in this thesis entitled "Synthesis and characterization of doped and undoped ZnS thin films using chemical bath deposition" by Ms. Saima Perveen, Registration No. 244-FBAS/MSPHY/S14 is of sufficient standard in scope and quality for the award of Degree of MS physics from International Islamic University, Islamabad.

**Committee**

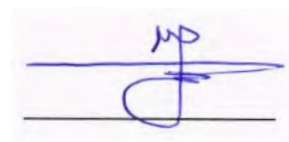
**External Examiner**

Dr. Zafar Iqbal,  
Professor and Head of Department,  
Department of physics,  
Riphah International University, Islamabad.



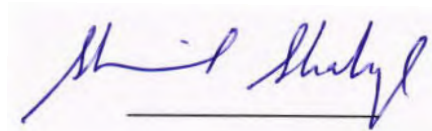
**Internal Examiner**

Dr. Naeem Ahmed,  
Assistant Professor,  
Department of physics,  
International Islamic University, Islamabad.



**Supervisor**

Dr. Shaista Shahzada,  
Assistant Professor,  
Department of physics,  
International Islamic University, Islamabad.



A thesis submitted to  
**Department of Physics,**  
International Islamic University, Islamabad  
As a partial fulfillment of requirement for the award of the degree of  
**MS physics**

## Declaration of Originality

I Saima Perveen, registration # 244-FBAS/MSPHY/S14 hereby declare that the work present in the following thesis is my own effort, except where otherwise acknowledged and that the thesis is my own composition. No part of the thesis has been previously presented for any degree. If the violation of HEC rules on research has occurred. I shall be liable to the disciplinary action under the plagiarism rules of Higher Education Commission (HEC), Pakistan.

Date: 31-08-2016

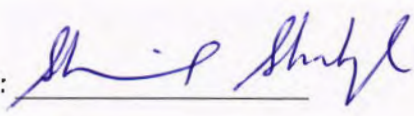


Signature: \_\_\_\_\_

Reg # 244-FBAS/MSPHY/S14

## Certificate

It is certified that Ms. Saima Perveen, Registration No. 244-FBAS/MSPHY/S14 has carried out the research work related to this thesis untitled "Synthesis and Characterization of Doped and Undoped ZnS Thin Films using Chemical Bath Deposition" under my supervision. This work fulfills all the requirements for the award of MS Physics.

Supervisor:   
Dr. Shaista shahzada



*Dedicated*

*To*

*My Great parents,*

*Grandparents, Teachers and siblings*

## Table of Contents

1.1 Thin films .....	1
1.1.1 Properties of Thin Films .....	1
1.1.2 Classification of Thin films .....	2
1.1.3 Defects .....	3
1.1.4 Applications:.....	3
1.2 Fabrication of thin films .....	3
1.3 Deposition Techniques .....	4
1.3.1 Physical Vapor Deposition.....	4
1.3.2 Chemical Vapor Deposition.....	4
1.4 Chemical bath deposition.....	5
1.5 Material .....	7
1.5.1 Zinc sulphide (ZnS): .....	7
1.5.1.1 Crystal Structure: .....	7
1.5.1.2 Crystal structure of zinc Sulphide:.....	8
1.5.1.3 Properties of ZnS .....	9
1.5.1.4 Applications: .....	10
1.5.2 Copper Chloride (CuCl <sub>2</sub> ): .....	11
1.5.2.1 Properties .....	11
1.5.2.2 Crystal Structure .....	11
1.5.2.3 Applications .....	12
1.5.3 Iron Chloride FeCl <sub>2</sub> .....	12
1.5.3.1 Properties .....	13
1.5.3.2 Applications .....	13
1.6 Literature survey.....	13
2.1 Experimental details.....	15

2.1.1 Growth of thin films .....	15
2.2 Characterization of thin films.....	18
2.2.1 X-Raydiffraction .....	18
2.2.2 Scanning electron microscopy (SEM) .....	20
2.2.3 Hall Effect measurements.....	22
2.2.4 Ultraviolet-Visible (UV-Vis) Spectroscopy.....	24
2.2.5 Ellipsometry.....	27
3.1 Structural analysis.....	30
4.1.1 Effect of temperature.....	30
4.1.2 Effect of deposition time.....	34
4.1.3 Effect of Doping in ZnS films.....	35
3.2 Morphological studies.....	37
3.2.1 Effect of temperature.....	37
3.2.2 Effect of deposition time.....	39
3.2.3 Effect of doping.....	41
3.3 Electrical properties .....	42
3.4 Optical properties through UV Vis Spectroscopy.....	44
3.4.1 Transmittance.....	39
3.4.2 Absorbance.....	41
3.4.3 Reflectance.....	43
3.4.4 Absorption coefficient.....	44
3.4.5 Energy band gap.....	49
3.4.6 Refractive index.....	52
3.4.7 Extinction coefficient.....	52
3.4.8 Real dielectric constant .....	54
3.4.9 Imaginary dielectric constant.....	56

3.4.10 Optical conductivity .....	57
3.5 Ellipsometry.....	61
3.5.1 Refractive index.....	61
3.5.2 Extinction coefficient.....	63
3.5.3 Real dielectric constant .....	64
3.5.4 Imaginary dielectric constant .....	66
3.5.5 Energy band gap.....	68
3.6 Conclusion.....	69
3.7 Future Prospects .....	69
References.....	70

## List of Figures

Figure 1.1: Structure of thin film.....	1
Figure 1.2: Typical steps in thin films .....	4
Figure 1.3: Schematic diagram of CBD .....	6
Figure 1.4 (a): Sphalerite (b) Wurzite.....	8
Figure 1.5: Prototypical structure of ZnS.....	8
Figure 1.6: Crystal structure of copper chloride.....	11
Figure 1.7: Crystal structure of Iron (II) chloride.....	12
Figure 2.1: Experimental step up.....	16
Figure 2.2 (a): Schematic diagram of brag's law.....	19
Figure 2.3: Schematic diagram of X-ray diffractometer .....	20
Figure 2.4: Schematic diagram of SEM.....	21
Figure 2.5: Illustration of Hall effect in abar of conducting material.....	23
Figure 2.6: Schematic diagram of single beam spectrometer.....	25
Figure 2.7: Electromagnetic spectrum.....	25
Figure 2.8: Graph of transmittance and concentration (beers law).....	27
Figure 2.9: Schematic diagram of ellipsometry experiment.....	28
Figure 3.1: XRD pattern of ZnS deposited at different temperature (a)T=32 <sup>o</sup> C (b)T=84 <sup>o</sup> C .....	30
Figure 3.2: XRD pattern of ZnS deposited at different deposition time .....	32
Figure 3.3: XRD pattern for Cu doped ZnS.....	33
Figure 3.4: XRD pattern for Fe doped ZnS.....	33
Figure 3.5: SEM micrographs for ZnS film deposited at different temperature (a) 32 <sup>o</sup> C (3 hrs) (b) 84 <sup>o</sup> C (3 hrs.) .....	34
Figure 3.6: EDX result of ZnS film .....	35
Figure 3.7: SEM micrographs for ZnS films deposited at deposition time (a) 1:30 hrs (b) 2 hrs (c) 2:30 hrs .....	36
Figure 3.8: SEM micrographs for doped ZnS film (a) Cu doped ZnS (b) Fe doped ZnS .....	37
Figure 3.9: I-V curves of samples.....	38
Figure 3.10: I-V curve of sample.....	38
Figure 3.11: Transmittance graph for ZnS deposited at different temperature (3 hrs.) .....	39
Figure 3.12: Transmittance graph for ZnS deposited for different deposition time (84 <sup>o</sup> C) .....	40
Figure 3.13: Transmittance graph for dopes ZnS films with Cu and Fe .....	40

Figure 3.14: Absorbance graph for ZnS deposited at different temperature (3hrs).....	41
Figure 3.15: Absorbance graph for ZnS deposited at different deposition time (84 <sup>0</sup> C).....	42
Figure 3.16: Absorbance graph for doped ZnS with Cu and Fe .....	42
Figure 3.17: Reflectance graph of ZnS deposited at different temperature (3 hrs) .....	43
Figure 3.18: Reflectance graph of ZnS deposited at different deposition time (84 <sup>0</sup> C) .....	43
Figure 3.19: Reflectance graph of doped ZnS with Cu and Fe.....	44
Figure 3.20: Absorption coefficient graph of ZnS at different temperature (3hrs) .....	46
Figure 3.21: Absorption coefficient graph of ZnS deposited at different deposition time (84 <sup>0</sup> C).....	46
Figure 3.22: Absorption coefficient graph for doped ZnS with Cu and Fe .....	47
Figure 3.23: Band gap values of ZnS films deposited at different temperature(3 hrs.) .....	48
Figure 3.24: Band gap values of ZnS films deposited at different deposition time(84 <sup>0</sup> c) ....	49
Figure 3.25: Band gap values of undoped and doped ZnS with Cu and Fe.....	49
Figure 3.26: Plot of refractive index vs wavelength $\lambda$ of ZnS thin films deposited at different temperature (3 hrs).....	50
Figure 3.27: Plot of refractive index vs wavelength $\lambda$ of ZnS thin films deposited at different deposition time (84 <sup>0</sup> C) .....	51
Figure 3.28: Plot of refractive index vs wavelength $\lambda$ for doped ZnS with Cu and Fe .....	51
Figure 3.29: Extinction coefficient graph for ZnS at different temperature(3hr).....	52
Figure 3.30: Extinction coefficient graph for ZnS at different deposition time (84 <sup>0</sup> C).....	53
Figure 3.31: Extinction coefficient graph for doped ZnS with Cu and Fe .....	53
Figure 3.32: Real dielectric constant graph for ZnS deposited at different temperature (3 hrs.) .....	54
Figure 3.33: Real dielectric constant graph for ZnS deposited at different deposition time (84 <sup>0</sup> C).....	56
Figure 3.35: Imaginary dielectric constant for ZnS deposited at different temperature (3 hrs) .....	56
Figure 3.36: Imaginary dielectric constant for ZnS deposited at different deposition time (84 <sup>0</sup> ) .....	56
Figure 3.37: Imaginary dielectric graph for doped ZnS with Cu and Fe .....	57
Figure 3.38: Optical conductivity graph for ZnS at different temperature (3 hrs) .....	57
Figure 3.39: Optical conductivity graph for ZnS deposited at different deposition time (84 <sup>0</sup> C) .....	58
Figure 3.40: Optical conductivity graph for doped ZnS with Cu and Fe .....	58

Figure 3.41: Plot of refractive index vs wavelength $\lambda$ of ZnS thin films deposited at different temperature (3 hrs) from ellipsometry .....	59
Figure 3.42: Plot of refractive index vs wavelength $\lambda$ of ZnS thin films deposited at different deposition time(84°C) from ellipsometry .....	60
Figure 3.43: Plot of refractive index vs wavelength $\lambda$ for undoped and doped ZnS thin films with Cu and Fe from ellipsometry .....	60
Figure 3.44: Extinction coefficient graph for ZnS at different temperature (3 hr) from ellipsometry.....	61
Figure 3.45: Extinction coefficient graph for ZnS at different deposition time (84°C) from ellipsometry.....	61
Figure 3.46: Extinction coefficient graph for undoped and doped ZnS with Cu and Fe from ellipsometry.....	62
Figure 3.47: Real dielectric constant graph for ZnS deposited at different temperature (3 hrs) from ellipsometry.....	63
Figure 3.48: Real dielectric constant graph for ZnS deposited at different deposition time (84°C) from ellipsometry .....	63
Figure 3.49: Real dielectric graph for undoped and doped ZnS with Cu and Fe from ellipsometry.....	64
Figure 3.50: Imaginary dielectric constant for ZnS deposited at different temperature (3 hrs) from ellipsometry .....	65
Figure 3.51: Imaginary dielectric constant for ZnS deposited at different time (84°C) from ellipsometry.....	65
Figure 3.52: Imaginary dielectric graph for doped ZnS with Cu and Fe.....	66
Figure 3.53: Band gap values of ZnS films deposited at different temperature(3 hrs.) from ellipsometry .....	66
Figure 3.54: Band gap values of ZnS films deposited at different deposition time(84°C) ....	67
Figure 3.55: Band gap values of undoped and doped ZnS with Cu and Fe from ellipsometry .....	68

## List of Tables

Table 1.1: Percentage Analysis.....	8
Table 1.2: Chemical Properties of ZnS.....	9
Table 1.3: Electrical Properties of ZnS.....	9
Table 1.4: Thermal Properties of ZnS.....	9
Table 1.5: Optical Properties of ZnS.....	9
Table 1.6: Mechanical Properties of ZnS.....	10
Table 1.7: Percentage Analysis Of CuCl <sub>2</sub> .....	12
Table 2.1: Deposition # 1.....	16
Table 2.2: Deposition # 2.....	17
Table 2.3: Deposition # 3.....	17
Table 2.4: Deposition # 4.....	17
Table 3.1: Structural Parameters of ZnS films calculated through XRD measurement.....	31
Table 3.2: Structural Parameters of doped ZnS films calculated through XRD measurement.....	33
Table 3.3: Atomic percentage in ZnS Films.....	35
Table 3.4: Comparison of thickness of ZnS films calculated by UV-Vis transmission & ellipsometry.....	45
Table 3.5: Comparison of thickness for doped ZnS films calculated by UV-Vis transmission & ellipsometry.....	45
Table 3.6: Band gap values of ZnS Films.....	47
Table 3.7: Band gap values of ZnS Films.....	48
Table 3.8: Band gap Of undoped and doped ZnS Films.....	49
Table 3.9: Comparison of Band gap values of ZnS Films from ellipsometry & UV-Vis spectroscopy.....	66
Table 3.10: Comparison of Band gap values of ZnS Films from ellipsometry & UV-Vis spectroscopy.....	67
Table 3.11: Comparison of Band gap Of undoped and doped ZnS Films from ellipsometry & UV-Vis spectroscopy.....	68



## Abstract

Nanocrystalline thin films of pure ZnS were deposited on the glass substrate by a chemical bath deposition method (CBD). Thin films of doped ZnS with Fe and Cu were also deposited by CBD method on a glass substrate. Different parameters e.g. temperature during reaction and time of deposition were changed during the growth. X-ray diffraction confirm the cubical zinc blende phase of pure ZnS. Whereas in the case of doping, change in structure is observed i.e. its lattice constant, d-spacing and grain sizes were changed. Optical properties of the films such as transmission, absorbance, reflectance, refractive index, real dielectric constant, imaginary dielectric constant, absorption coefficient, extinction coefficient, optical conductivity and band gap were determined through the UV-Vis spectrum and ellipsometry. Optical measurements reveal that all the samples have maximum transmission in wavelength above 350nm with a band gap varying between 3.6 eV to 3.8 eV for pure ZnS films and in case of doping band gap changed to 3.89 eV. I-V curves have been observed through electrical characterization. SEM images reflect the growth of clusters and tube like structures in case of doping of ZnS films, whereas in remaining all pure ZnS films show granular structures.

## Acknowledgment

First of all my all praises and thanks are for Allah Almighty who blessed me and granted me the strength to complete this project successfully. This journey would have not been possible without the guidance of my teachers, help and support from my family and friends.

I extend my sincere and humble thanks to my supervisor, Dr. Shaista Shahzada for his guidance, encouragement and for grooming me as M.S student.

My special thanks is also to Mr. Imran from F.U.U.A.S.T for helping me through my difficulties, for his support and patience during writing process.

I am also grateful to the Head of Environmental science Department, Dr. Maliha Asma & Sir Shoaib for providing the lab facilities and Guidance. I would like to acknowledge the authorities of PIEAS Lab, IST and IDB Lab (IIU) for providing me opportunity to avail the facilities related to my Research.

I am obliged to all my friends who were always there for me, and special thanks to Aisha, Shafa Ashraf and Najam-ul-Athar Rayma for sharing their knowledge.

Last but not the least, I am indebted to my family; my parents, grandparents and siblings who gave me inner strength and encouraged me with their best wishes. Thank you all for your unconditional love, support and unwavering belief in me.

Special thanks are for my father, Manazir Hussain Abbasi, who always stands with me in every difficult time, thank you for being the person who always says 'let's see how we can fix this' instead of 'I tell you to do like this'.



Saima Perveen

## Chapter 1 Introduction

A microscopically thin layer of material that is deposited on a metal, ceramic, semiconductor or plastic base, typically less than one micron thick is known as thin films. Thin films can be conductive or dielectric (non-conductive) and are used in myriad applications [1]. For example, the top metallic layer on a chip and the coating on magnetic disks are thin films. Let's have a brief outlook on thin films firstly.

### 1.1 Thin films

Thin films are meant to be layers, their thickness is ranging from micrometer to nanometer. There are several different notations of thin films in science and engineering. For example, the meaning of thin film may be denoted as laminated viscous layer of a fluid. A typical structure of thin film is illustrated in figure

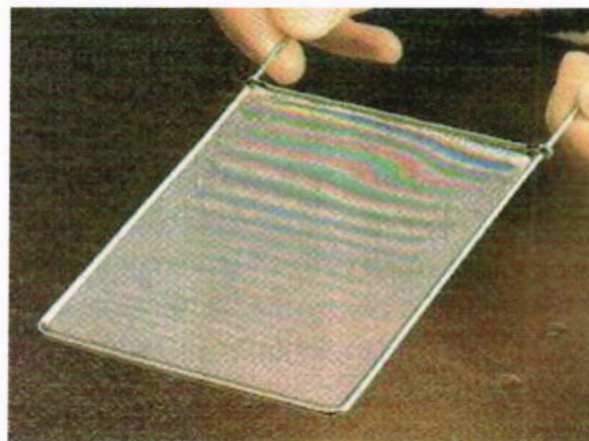


*Figure 1.1: Structure of thin film*

Thin films have different properties as compared to bulk material with which they are made of. Now we summarize these properties of thin films.

#### 1.1.1 Properties of Thin Films:

Thin films properties are different from bulk materials. Thin films may be

- Not fully dense.
- They are ranging from monolayer to several micrometers
- Quantum confinement effect can be observed in thin films
- Thin films are often under stress

- Thin films have defect structures different from bulk
- These are quasi - two dimensional structure (very thin films)
- Different properties are strongly influenced by surface and interface effects

This will change electrical, magnetic, optical, thermal, and mechanical properties. Thin films are the key element of continued technological advances made in the fields of optoelectronic, photonic and magnetic devices. Their studies have directly or indirectly advanced many new areas of research in solid state physics and chemistry which are based on phenomena uniquely characteristic of the thickness, geometry and structure of the film. The processing of materials into thin films allows easy integration into various types of devices.

Thin films are thermally stable and reasonably hard, but could be fragile. Their mechanical properties can be measured by tensile testing of freestanding films and by micro beam cantilever deflection technique, but the easiest way is by means of Nano-indentation. Optical characterization provides a good way of examining the properties of semiconductors. Particularly measuring the absorption coefficient for various energies gives information about the band gaps of the material.

### 1.1.2 Classification of Thin films

Thin films are classified in many ways mainly, according to the materials used for coatings, the damage threshold and strength, etc. Thin film technology has been developed primarily for the need of the integrated circuit industry. Thin films as a two dimensional system are of great importance to many real-world problems. Their material costs are very small as compared to the corresponding bulk material and they perform the same function when it comes to surface processes. Thin film technology is based on three foundations:

- Fabrication
- Characterization
- Applications.

Some of the important applications of thin films are microelectronics, communication, optical electronics, and catalysis, coating of all kinds, and energy generation and conservation strategies. Manufacturing of many machine parts require thin film coating of different materials i.e. carbides and nitrates because they are used to harden and protect cutting and sliding surfaces. Wear characteristics of metal surfaces are improved by these various coatings [2]. Thin film science and technology plays an important role in the high-tech industries. In the

history of thin films, defects are very important and play a vital role. Importance of defects is illustrated as follows

### 1.1.3 Defects

Nanostructure is converted to microstructure in the presence of some defects like vacancies interstitial, impurities, deformed bond and surface roughness etc. Structural defects like dislocations determine the mechanical properties of materials. The local distortions of the atomic lattice in the vicinity of the dislocation influence the mechanical strength. Defects can affect the properties of thin films as spatial fluctuation of the atomic composition, variation in granular structure involving size, grain boundaries and thickness etc. Thin films have number of application in different fields. Few of these are listed below

### 1.1.4 Applications

Thin films play vital role in different applications field like

- ❖ Optics (Anti-reflection, Anti-reflection coating; on lenses or solar cells, Reflection coatings for mirrors etc.)
- ❖ Chemistry (sensors for liquid, diffusion barriers, protection against corrosion etc.)
- ❖ Magnetics (video/audio tapes, hard disks etc.)
- ❖ Electricity without semiconductors (conducting films for resistor, capacitors etc.)
- ❖ Mechanics (friction reduction, adhesion providers etc.)
- ❖ Electronics (LEDs ,LCDs)
- ❖ Tailored materials. (Layer very thin films to develop materials with new properties etc.)

Thin film materials are used in semiconductor devices, wireless communications, telecommunications, integrated circuits, rectifiers, transistors, solar cells, light-emitting diodes, photoconductors and light, crystal displays, lithography, micro- electromechanical systems (MEMS) and multifunctional emerging coatings, as well as other emerging cutting technologies.

## 1.2 Fabrication of thin films

Typical steps that are involved in manufacturing of thin film are as follows

1. Emission of particles from source (through heat, high voltage)

2. Transport of particles to substrate (free vs. directed)
3. Condensation of particles on substrate (how do they condense)

These steps were illustrated in a simple model form in the figure

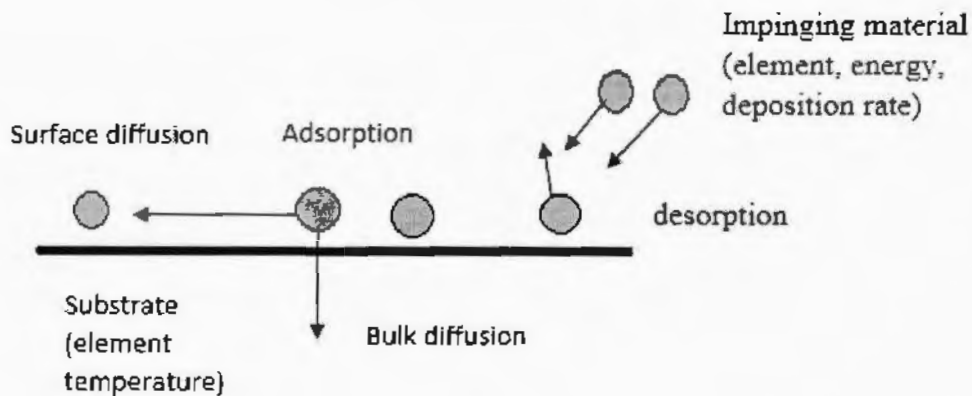


Figure 1.2: Typical steps in thin films

During the fabrication process of thin films, deposition techniques play a vital role. Different deposition techniques are used to deposit thin films. Some of them are as

### 1.3 Deposition Techniques

Thin film deposition is the process by which we can produce a thin film on to a surface. These surfaces on which films are deposited are called substrate. We also come across the cases where thin films are deposited on already grown films. Importance of film deposition more enhance in case of better understanding and for the measurement of optical, structural and electrical properties. There are different deposition techniques based on physical or chemical processing.

#### 1.3.1 Physical vapor Deposition

Different techniques of physical vapor deposition are as follows

- Sputtering
- Thermal Evaporation
- Pulsed laser Evaporation
- Molecular beam epitaxy(MBE)
- Plasma process

#### 1.3.2 Chemical vapor Deposition

Similarly some of the techniques based on the chemical vapor deposition are listed below

- Thermal oxidation
- Electroplating
- Plasma enhanced(PE) CVD
- Ion implantation
- Liquid phase epitaxy
- Photon activated CVD
- Laser induced CVD
- Chemical bath deposition (CBD)

We used chemical bath deposition method to deposit our thin films in the reported project

### **1.4 Chemical bath deposition (CBD)**

First of all Bunsen and Grove obtained metal films in 1852 by means of chemical deposition and flow discharge of sputtering, respectively. Faraday made metal films in 1857 by the thermal evaporation on explosion of current carrying metal wire. The usefulness of the optical properties of metal films and the scientific curiosity about the behavior of two dimensional solids has been responsible for the immense interest in the study of science and technology of thin films.

The Chemical bath deposition (CBD) method is one of the cheapest methods to deposit thin films and nanomaterials. The main purpose of depositing thin films using CBD (chemical bath deposition method) is that, it can be employed for large area batch processing or continuous deposition. This method is also popular due to some of its amazing properties such as it is non-polluted, less expensive instruments, simple in operation, use low temperature like room temperature, last but not least the materials which we used are easily available in the market. Some other advantages that are present in this method are as it is versatile method, easy to handle, no need of vacuum, no inert gas required, less cost and high yield. CBD is basically based on the formation of a solid phase from a solution [3]. The chemical bath deposition involves two steps,

- Nucleation
- Particle growth

Experimental arrangement for chemical bath deposition method is illustrated in figure 1.3.

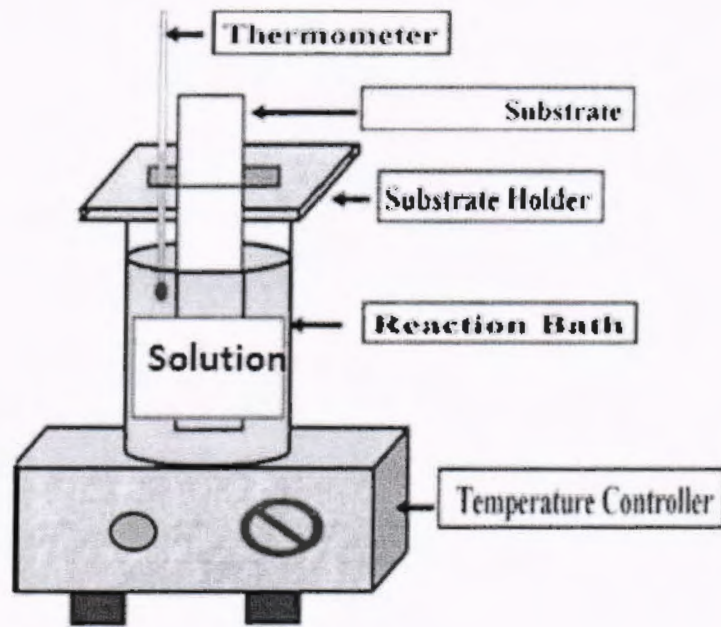


Figure 1.3: Schematic diagram of CBD

This is based on the formation of a solid phase from a solution. In the chemical bath deposition procedure, the substrate is immersed in an aqueous solution containing the precursors. Generally the whole process of CBD can be summarized as follows

- Prepare the solution of precursor according to the required film,( to be deposited)
- Introduce this solution inside the beaker
- Next, the substrate was immersed in the solution
- Put the whole assembly on a magnetic heat stirrer for deposition of films.

Chemical bath deposition method also have some other important uses, which are as CBD method require a simple apparatus for the deposition of thin film. The equipment used has a lower cost compared with other method. One of the major advantages of CBD is that it requires in its simplest form only solution containers and substrate mounting devices. One of the drawbacks of this method is the wastage of solution after every deposition. Chemical bath deposition yields stable, adherent, uniform and hard films with good reproducibility by a relatively simple process. The growth of thin films strongly depends on growth conditions, such as

- Duration of deposition
- Composition of film.
- Temperature of the solution.



- Topographical of film.
- Chemical nature of the substrate

Different combinations of materials are used to deposit films of ZnS. The materials that we used to deposit our thin films of ZnS are as

## 1.5 Materials

Thin films of different materials were prepared and analyzed. In our proposed research work we required II-VI materials. Detail of these materials are summarized as

### 1.5.1 Zinc Sulphide (ZnS)

CdS buffer layer is most widely used in thin films solar cell [4]. But Cd is toxic and can cause serious environmental problems. So nowadays Zinc sulfide (ZnS) is becoming more important and considered to be as a promising candidate for replacement of toxic CdS in the buffer layer for CIGS solar cells. ZnS has several advantages over CdS in application range i.e.

- A solar cell with ZnS as buffer layer has been realized with efficiency of 18.6% [5].
- ZnS films can increase responses in short wavelength region.
- ZnS films can also reduce the band offset of the ZnS/ZnO layer, because the ZnS bandgap (3.5-3.7 eV) is close to ZnO bandgap (3.7 eV).

ZnS with the addition of few suitable activator such as phosphorous, it can be used as luminescent material. It also has many advantages such as

- It is an important semiconductor with direct band gap and high refractive index.
- Relatively cheaper and abundant
- Optical properties of ZnS can be tuned easily by modulation of their size, chemical composition and impurity(defects) doping [6]

#### 1.5.1.1 Crystal Structure

ZnS is an inorganic compound with the chemical formula ZnS. It mainly occurs in the minerals sphalerite and wurtzite. Both sphalerite and wurtzite are intrinsic, semi-conductors-, wide band gap. In its dense form, zinc sulfide can be transparent. ZnS exists in two main crystalline forms, in each form, the coordination geometry at Zn & S is tetrahedral. The more stable cubic form is zinc blende & hexagonal form is know is the mineral wurzite. Structure of zinc blende and wurzite are illustrated in figures

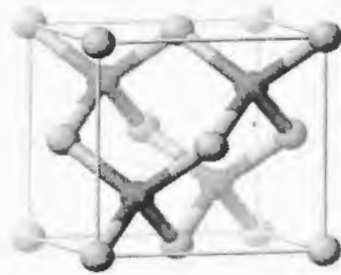


Figure 1.4 (a): Sphalerite

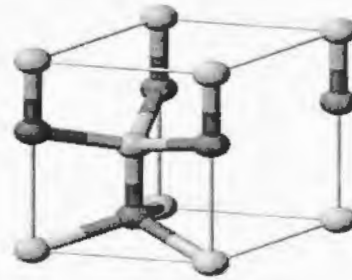


Figure 1.4 (b): Wurzite

Both zinc blende & wurzite are intrinsic, wide-bandgap semi-conductors. The cubic form of ZnS has a band gap of about 3.54 eV, but the hexagonal form has a band gap of about 3.91 eV in direct region. ZnS occurs naturally as "zinc blend," and is prepared directly from the elements and by precipitation of a zinc salt solution with ammonium sulfide. It is produced at a relatively low cost so many of its applications are as a substitute for other materials. ZnS is a gray or off white powder that is insoluble in water, but soluble in acid.

### 1.5.1.2 Crystal structure of zinc Sulphide:

Element analysis of zinc sulphide is shown in table 1.1.

Table 1.1: Percentage Analysis

Element analysis	%
Zn	67.10
S	32.90

Prototypical structure of Zinc Sulphide has arrangement of zinc and sulphide as shown in figure

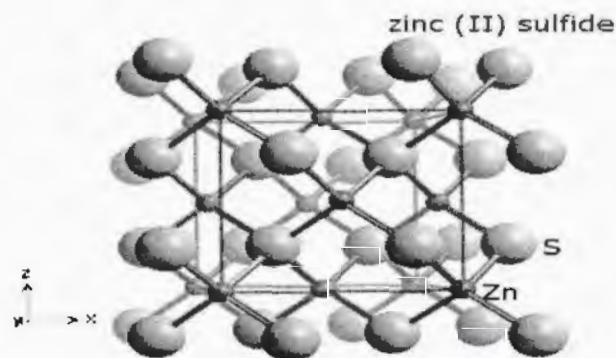


Figure 1.5: Prototypical structure of Zinc Sulphide

### 1.5.1.3 Properties of ZnS

ZnS properties that we are going to discuss here are as categorizing as chemical, electrical, thermal, optical and mechanical. All of these properties are summarize as [7]

*Table 1.2: Chemical Properties of ZnS*

Chemical properties	
Chemical Formula	ZnS
Molecular Weight	97.46
CAS No.	1314-98-3
Group	Zinc - 12 Sulfur - 16
Crystal Structure	Cubic
Lattice Constant	5.4093 Å

*Table 1.3: Electrical Properties of ZnS*

Electrical Properties	
Dielectric Constant	8.9
Band Gap	3.54 eV
Electron Mobility	180 cm <sup>2</sup> /Vs
Hole Mobility	5 cm <sup>2</sup> /Vs

*Table 1.4: Thermal properties of ZnS*

Thermal properties	
Heat of Fusion	390 J/g
Heat of Formation	477 kJ/mol
Thermal Expansion Coefficient	6.36 μm/m°C
Specific Heat Capacity	0.472 J/g°C
Thermal Conductivity	25.1 W/mK

*Table 1.5: Optical Properties of ZnS*

Optical properties	
Refractive Index	2.356

*Table 1.6: Mechanical Properties of ZnS*

Mechanical properties	
Density	4.079g/cm <sup>3</sup>
Density	
Melting Point	1850°C

Flexural Strength	103 MPa
Modulus of Elasticity	75 GPa
Poisson's Ratio	0.27
Mohs Hardness	3.8

#### 1.5.1.4 Applications:

Zinc sulfide is used as a friction material to carry sulfur, which hardens rotor surfaces and thereby reduces wear [8]. It is also used in printing inks, UV-hardened systems, powder coatings, adhesives, insulating & sealing compounds, thermoplastic pigmentation, thermosets, flame resistant plastics, glass-fiber reinforced plastics, pigment concentrates, elastomers, textile fibers, paper, mastics, lubricants, electroluminescent lamps, infrared windows, domes and optical elements.

ZnS thin films have also been found useful in various devices. The applications of ZnS thin films which cover a wide area of interest. Some of the uses are as

- Preparation of flexible transparent conductive coatings which are essential for fabrication of a variety of printed electronic devices such as flexible displays and solar cells
- Antireflection coating for the solar cell.
- Environmental friendly buffer layer as compared to CdS layer in CIS based thin film solar cell [9].
- Wide band gap material for electroluminescent and opto-electronic devices.
- Photosynthetic coatings [10].
- Blue light emitting laser.
- Particle detector [7].
- Catalyst

Zns can also be doped to improve the mechanical, electrical, optical or magnetic properties of thin films. These doped ZnS semiconductor materials have a wide range of applications in electro-luminescence devices, phosphors, light emitting displays, and optical sensors. We aim to dope ZnS thin films with copper and Iron. Following section briefly summarize the chemical used for doping.

## 1.5.2 Copper Chloride (CuCl<sub>2</sub>)

CuCl<sub>2</sub> is the chemical formula of the compound also known as copper (II) chloride. This is a light brown solid, which slowly absorbs moisture to form a blue-green dihydrate. The copper (II) chlorides are some of the most common copper (II) compounds, after copper sulfate. Copper (II) chloride is intrinsically paramagnetic [10].

Copper (II) chloride, also known as cupric chloride, forms a blue-green, orthorhombic, crystalline structure in the dehydrated state and can be used as (amongst other things) a flame colorant, oxidizing agent, and militant Lewis acid. It is highly soluble in water and will produce a blue solution, but when concentrated the CuCl<sub>2</sub> aqueous solution will turn dark green.

### 1.5.2.1 Properties

- **Chemical Formula:** CuCl<sub>2</sub>, CuCl<sub>2</sub>·2H<sub>2</sub>O
- **Odor:** odorless
- **Color:** blue-green solid
- **Melting point:** 422°C; 430°C
- **Boiling point:** 1490°C
- **Density:** 2.51 g/cm<sup>3</sup> (25°C relative to water at 4°C)
- **Specific Gravity:** 2.54 at 68.0 ° F (USCG, 1999)
- **Molar Mass:** 134.45 g/mol

### 1.5.2.2 Crystal Structure

Copper II chloride has structure same as sphalerite structure of zinc sulphide. The crystal structure of copper II chloride is shown.

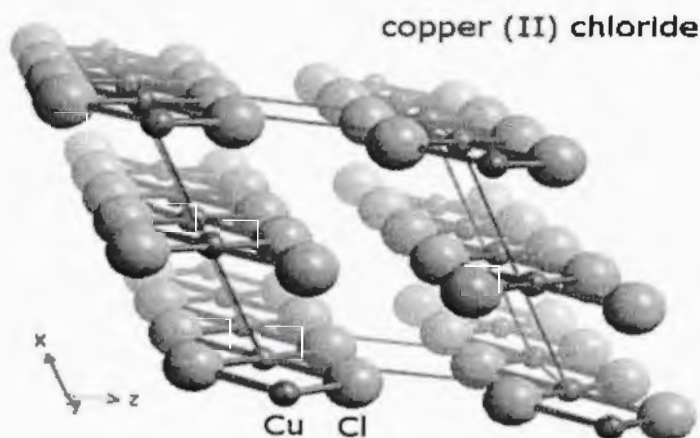


Figure 1.6: Crystal structure of copper chloride

Whereas the element percentages in copper chloride is shown in table 1.8

Table 1.7: Percentage Analysis of  $\text{CuCl}_2$

Element	Percentage%
Cl	35.81
Cu	64.19

### 1.5.2.3 Applications

- It is used as a catalyst for organic and inorganic reactions, mordant for dyeing and printing textiles.
- As a catalyst in the production of chlorine from hydrogen chloride [7].
- It is also used in the petroleum industry as a purifying agent,
- In tinting baths for iron and tin, in photography, in pyrotechnics, and to remove lead
- It is used in wood preservative, disinfectant, insecticide, fungicide, and herbicide
- In metallurgy to recover mercury from ores, in refining copper, silver and gold
- As a pigment for glass and ceramics
- In the manufacture in indelible, invisible, and laundry marking inks.

### 1.5.3 Iron Chloride ( $\text{FeCl}_2$ )

$\text{FeCl}_2$  Iron (II) chloride, also known as ferrous chloride. It is a paramagnetic solid with a high melting point, and is usually obtained as an off-white solid.  $\text{FeCl}_2$  crystallizes from water as the greenish tetrahydrate, which is the form that is most commonly encountered in commerce and the laboratory. The compound is also soluble in water; aqueous solutions of  $\text{FeCl}_2$  are yellow. Its crystal structure is monoclinic as illustrated in figure 1.7.

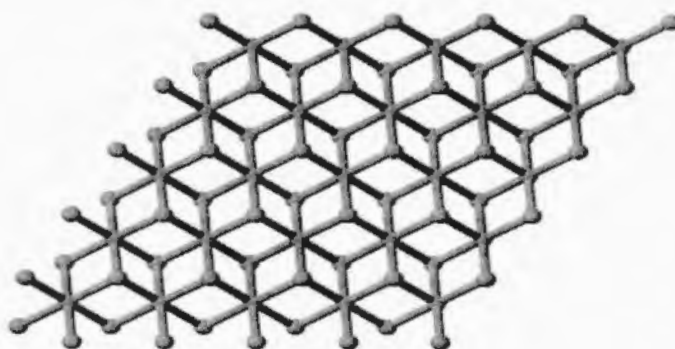


Figure 1.7: Structure of Iron (II) chloride

### 1.5.3.1 Properties

- **Chemical formula:**  $\text{FeCl}_2$
- **Color:** pale green
- **Molar mass:** 126.751 g/mol (anhydrous)  
198.8102 g/mol (tetrahydrate)
- **Density:** 3.16 g/cm<sup>3</sup> (anhydrous)  
2.39 g/cm<sup>3</sup> (dihydrate)  
1.93 g/cm<sup>3</sup> (tetrahydrate)
- **Melting point:** 677 °C (1,251 °F; 950 K) (anhydrous)  
120 °C (dihydrate)  
105 °C (tetrahydrate)
- **Boiling point :** 1,023 °C (1,873 °F; 1,296 K) (anhydrous)

### 1.5.3.2 Applications

Ferrous chloride has a variety of nice applications, but the related compounds ferrous sulfate and ferric chloride enjoy more applications. Its major uses are as follows:

- It is used in the laboratory for synthesis of iron complexes,
- Ferrous chloride serves as a reducing flocculating agent in wastewater treatment, especially for wastes containing chromate [7].
- It is the precursor to hydrated iron (III) oxides that are magnetic pigments [11].
- Ferrous chloride is employed as a reducing agent in many organic synthesis reactions.

## 1.6 Literature survey

Types II–VI semiconductors have long been developed as materials for optoelectronics. The band gap for these mixed-crystal semiconductors can be greatly varied simply by changing their composition, and these semiconductors are used as materials in light emitters of a range of wavelengths from the visible to the infra-red spectrum, as well as in photo acceptance units. Recently, types II–VI semiconductors have also been employed in the buffer layer of Cu (In,Ga)Se<sub>2</sub> (CIGS) thin-film solar cells. CIGS solar cells were typically fabricated using a cadmium sulfide (CdS) buffer layer in order to protect the junction region from sputtering damage during subsequent zinc oxide (ZnO) deposition and to modify the surface of CIGS

absorber [12]. However, the quantum efficiency of a CdS/CIGS solar cell drops at short wavelengths due to optical absorption losses from the CdS layer. This implies that further improvement in the short circuit current ( $J_{sc}$ ) can be achieved by replacing CdS with another appropriate wider band gap buffer material. In addition to these technical considerations, avoiding the use of cadmium compounds is desirable from the viewpoint of environmental safety.

One promising alternative material is ZnS thin film. Its band gap energy ( $E_g$ ) of 3.68 eV at room temperature [13] makes it transparent to practically all wavelengths of the solar spectrum. In contrast CdS, with its band gap of 2.42 eV at room temperature [14], is highly absorbing for wavelengths below 520nm [15]. There has been a considerable progress in using ZnS in CIGS thin-film solar cells, ZnO/ZnS/CIGS solar cells with efficiency of up to 18.6% have been fabricated [16].

A very attractive method for producing ZnS thin films, due to the possibility of large-area deposition at low cost is the so-called chemical bath deposition (CBD) method [17, 18]. Ammonia and hydrazine are popular choices as the complexing agent in the CBD of ZnS thin films. For instance, Dona and Herrero [19] have deposited ZnS films using hydrazine hydrate as a complexing agent. However, the films obtained by CBD method are either amorphous or poorly crystallized. Therefore, annealing at high temperature was needed to improve the crystallinity of the thin films [20]. In addition, tri-sodium citrate can significantly improve the quality of the ZnS films obtained [21]. Go'de et al. obtained hexagonal ZnS thin films using triethanolamine and tri-sodium citrate as complexing agents by CBD at 84°C with 4.5 h [13]. Chemical deposition of ZnS films has been carried out in aqueous alkaline baths by many workers [22-25]. In our work ZnS thin films had been deposited by chemical bath deposition (CBD) method onto glass substrates.



## Chapter 2 Growth & Characterization of Films by Chemical Bath Deposition

We used chemical bath deposition method to deposit our thin films due to its intrinsic properties like simple process. Experimental detail of our process is as follows.

### 2.1 Experimental details

We have divided our experimental work in three steps

- i. Deposition of un-doped thin films of ZnS by using CBD.
- ii. Deposition of Cu and Fe doped thin films of ZnS using FeCl<sub>2</sub> and CuCl<sub>2</sub> materials.
- iii. Characterization of thin films using different techniques like XRD, SEM, UV-Vis Spectroscopy, ellipsometry, I-V measurements through two-probe electrical measurement technique.

Details of all above mentioned steps are given in the following sections

#### 2.1.1 Growth of thin films

The reaction between zinc chloride (ZnCl<sub>2</sub>) and thiourea (CS(NH<sub>2</sub>)<sub>2</sub>) laid the base for the formation of thin films of ZnS by using CBD technique. The corresponding reaction is as follows



For initially above reaction we have taken 20ml of 0.4M solution of ZnCl<sub>2</sub> by adding 1.09g of ZnCl<sub>2</sub> in 20ml of distilled water, then it is added to an excess of aqueous ammonium to form white precipitates of [Zn(NH<sub>3</sub>)<sub>4</sub>]<sup>2+</sup> which on stirring dissolve completely to form a clear solution. Then to this solution 13ml of 0.6M solution of CS(NH<sub>2</sub>)<sub>2</sub> was added, which was prepared by adding 0.45g of CS(NH<sub>2</sub>)<sub>2</sub> in 13ml distilled water and stirred for three hours. Finally in order to form an alkaline medium for deposition to take places 10ml of 0.15M solution of NaOH was added. This NaOH solution was prepared by adding 0.059g of NaOH in 10ml distilled water.

Glass substrates were then immersed vertically in to the solution and films were deposited. Experimental setup is illustrated in the figure 2.1.

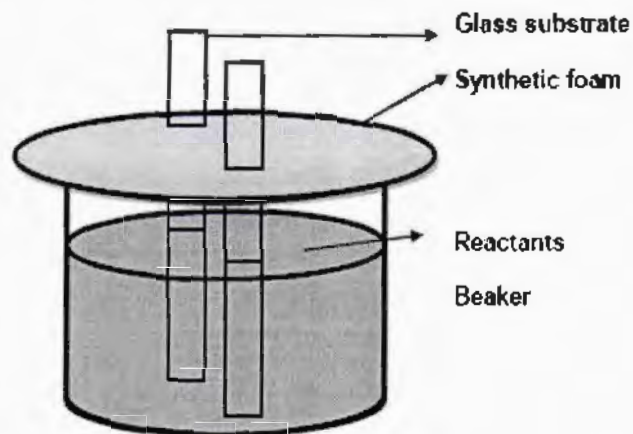


Figure 2.1: Experimental Set-up

In each batch four slides were immersed in the solution. Many samples were deposited under different set of conditions such as temperature of solution, growth time and pH of solution.

### Deposition # 1

Optimum depositions were observed on the slides immersed in the beaker. In our first case we changed the temperature of the solution and deposited thin films of ZnS on glass substrate at two different temperatures. Remaining conditions for this deposition are as follows

Table 2.1: Deposition # 1

Samples	Temperature	PH of solution	Deposition Time
ZnS	32°C	9	3 Hours
ZnS	84°C	5	3 Hours

We tried to optimize the process by changing different parameters of the process e.g temperature of the bath, deposition time and pH of solution.

### Deposition #2

In second case, we changed the growth time of the ZnS thin films on glass substrate and deposited thin film on glass substrate at different time interval.

Remaining deposition conditions in this case are as follows

*Table 2.2: Deposition # 2*

Samples	Temperature	PH of solution	Deposition Time
ZnS	84°C	5	1:30 Hours
ZnS	84°C	5	2:00 Hours
ZnS	84°C	5	2:30 Hours
ZnS	84°C	5	3:00 Hours

### Deposition #3

In third case, we doped copper in ZnS thin film by adding 20ml of 0.4M solution of copper chloride ( $\text{CuCl}_2$ ) in the same final solution that are used to deposited un-doped ZnS thin films. This solution of copper chloride was prepared by adding 1.07g of copper chloride ( $\text{CuCl}_2$ ) in 20ml of distilled water. Others conditions in this case are as shown in table 2.3.

*Table 2.3: Deposition # 3*

Sample	Temperature	PH of solution	Deposition Time
Cu doped ZnS	84°C	5	3 Hours

### Deposition #4

In final case, we doped iron in ZnS thin film by adding 20ml of 0.4M solution of iron chloride ( $\text{FeCl}_2$ ) in the same final solution that are used to deposited un-doped ZnS thin films. This solution of iron chloride was prepared by dissolving 1.014g of iron chloride ( $\text{FeCl}_2$ ) in distilled water. Others conditions in this case are as shown in table 2.4.

*Table 2.4: Deposition # 4*

Samples	Temperature	PH of solution	Deposition Time
Fe doped ZnS	84°C	5	3 Hours

After preparation of all these samples by above mention process, samples of prepared thin films were subjected for the characterization.

## 2.2 Characterization of thin films

After deposition process, prepared thin films were taken for characterized for their structural, optical and electrical behavior. Detail of the different techniques used in our experiment is elaborated in the proceeding sections.

### 2.2.1 X-Ray diffraction measurement

X-Rays are electromagnetic radiations. XRD is employed, when X-Rays falls on the surface of the material. This X-Ray beam is not only absorbed by or transmitted, but also a part of it is scattered. The incident X-Ray beam interacts with the different planes of atoms and diffract by crystal planes, which is recorded on the film.

Crystalline structure and composition of different types of samples like thin films, powders and substrates can be determined by X-Ray diffraction (XRD) technique. X-Ray diffraction technique is a non-destructive technique. We use it to determine the crystalline phase which is present in the sample. A variety of other parameters can also be determined by using X-Ray diffraction. It determines variety of structural parameters such as grain size, phase composition, preferred orientation and defect in structure along with strain.

In crystalline materials, atoms are arranged in periodic manner. In each crystal, there is a unit cell describing the properties of the material. Crystal possess a repetitive, regular internal structure [26]. The concept of symmetry, describe the repetition of structural features. At regular interval in crystal, there exist parallel planes. These parallel planes are associated to the direction and distances in the crystal. These intervals are known as “cell constant” such as a, b and c. Orthogonal coordinate system is based upon these constants.

Indexing is a process of determining the unit cell parameters from peak positions. To index a powder diffraction pattern it is necessary to assign Miller indices (h, k, l) corresponding to each peak. Miller indices are basically an arbitrary set of planes and it define where the plane intersects the coordinate axes in integer multiples of a, b and c respectively. The distance d between hkl planes in a cubic crystal, for which a=b=c is known as d-spacing. For cubic phase the d-value can be calculated from Miller indices (hkl), using the following relation

$$d_{hkl} = \frac{a}{\sqrt{h^2+k^2+l^2}} \dots\dots\dots (2.1)$$

In XRD, during this scattering process from a crystal lattice, a peak of scattered intensity are observed which corresponds to the following conditions

- Angle of incidence = Angle of scattering
- The path length is equal to an integer number of wave lengths

Between the X-Ray source and the sample, there exists an angle known as “incident angle”, while the diffracted angle ( $2\theta$ ) is the angle between the incident ray and the detector angle. These angles were illustrated in figure

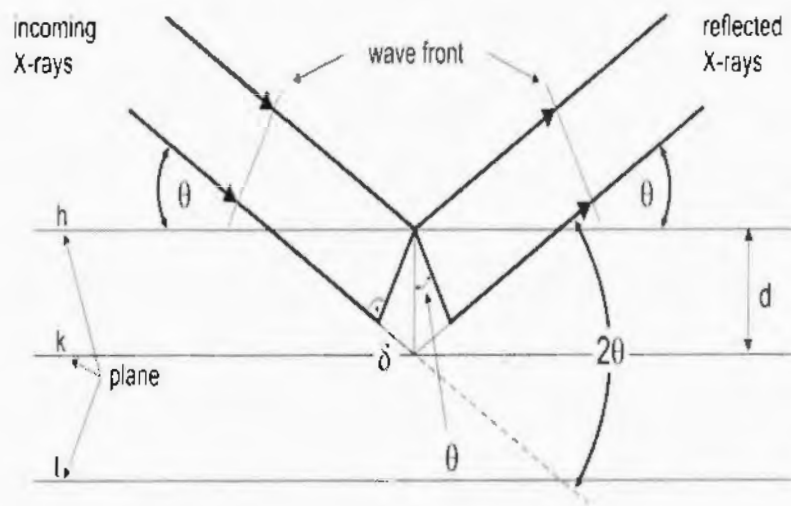


Figure 2.2: Schematic diagram of bragg's law

The condition for maximum intensity contained in Bragg's law allow us to calculate details about crystal structure. If the crystal structure is known, and constructive interference of X-Rays occurs at the detector then the wavelength of X-Rays incident upon the crystal from planes of spacing  $d$  is

$$n\lambda = 2d\sin\theta \dots \dots \dots (2.2)$$

$\theta$  is the angle between atomic planes and diffracted beam and  $n$  is a positive integer representing the order of reflection

XRD require relatively small time for data acquisition. A good spectrum or lattice parameter measurement can be obtained from test of 10 – 30 minutes. XRD provides structure information about the whole sample, more ever it requires a little sample preparation. For XRD analysis, an X-Ray diffractometer is use. Its structure is illustrated in figure

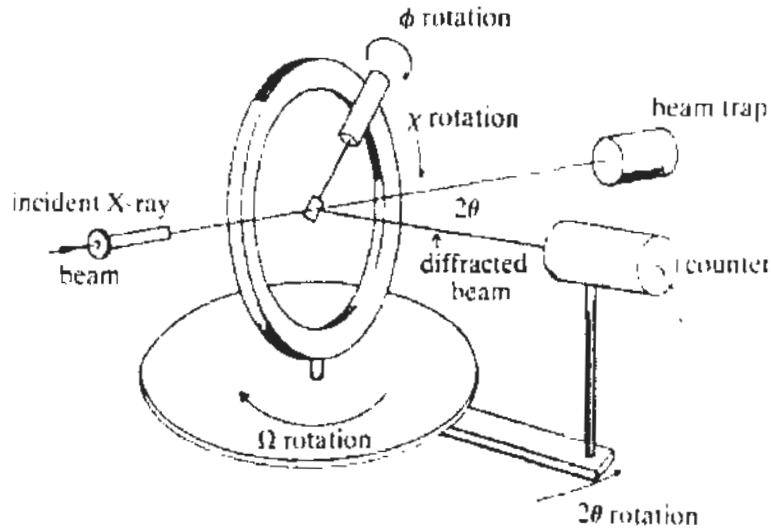


Figure 2.3: Schematic diagram of X-ray diffractometer

The determination of an unknown structure from diffraction pattern proceeds in following [7]

- The shape and size of a unit cell are deduced from the angular positions of the diffraction line
- The number of atoms per unit cell is then computed from the shape and the size of the unit cell, chemical composition of the sample, and its measured density
- Finally the position of atom within the unit cell are deduced from the relative intensities of the diffraction lines

The third step is generally the most difficult as there are many structures which are known incompletely. This step is same as the indexing of powder diffraction pattern as it involves

- The accurate determination of peak positions
- Determination of unit cell parameters from the peak positions

### 2.2.2 Scanning Electron Microscopy (SEM)

One of the most widely used techniques in characterization of nanomaterials and nanostructures is SEM, whose resolution approaches a few nanometers. The magnifications of SEM instrument are also easily adjusted from- 10 to over 3000,000.

Principle of SEM is that it uses focused beam of electrons scanning over the surface specimens (thick or thin specimens). Finally images are produced one spot at a time in a grid-like raster pattern. Not only does the SEM provides us topographical information as optical microscopes

do, it also provides the chemical composition information near the surface of sample. A schematic diagram of scanning electron microscope is illustrated in figure 2.4.

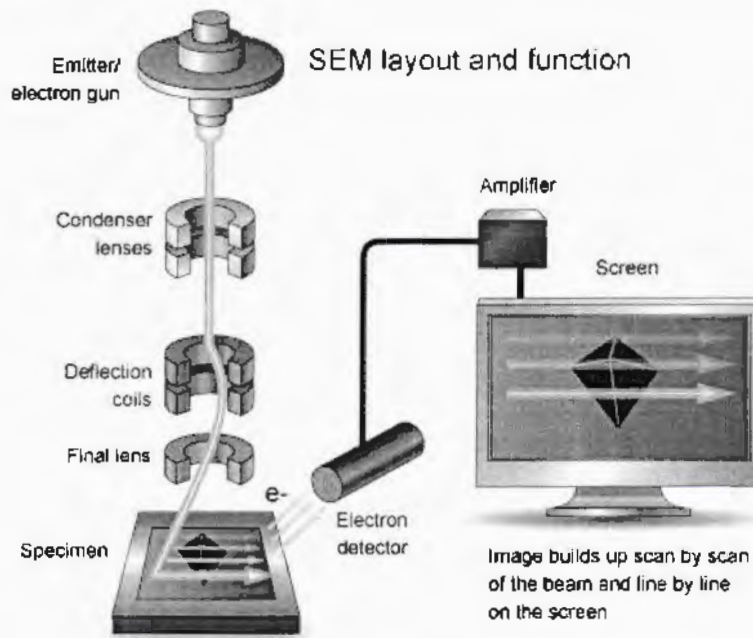


Figure 2.4: Schematic diagram of SEM

In SEM a beam strikes the sample, dwells for few seconds. Interactions occur inside the sample and are detected with various instruments. During SEM inspection, a beam of electrons is focused on a spot volume of the specimen. This beam resulting in the transfer of energy to the spot. These bombarding electrons (also referred to as primary electrons) dislodge electrons from the specimen itself. The dislodged electrons (also known as secondary electrons) are attracted and collected by a positively biased grid or detector. Which is finally converted into a signal [27]. On the basis of what is subsequently detected and imaged, SEM techniques can be differentiated with others. The principle images produced in the SEM are of three types:

- Backscattered electron images
- Elemental X-ray maps
- Secondary electron images

SEM images give us the detail information about sample

- Topography  
(The surface features of the specimen, e.g its texture; thus direct relation between these features and material properties)

- Morphology  
(The shape and size of the particles with which the specimen is made up of; direct relation between these structures and material properties)
- Composition  
(The relative amount and detection of elements and compounds that the specimen is composed of; thus direct relation between composition and material properties)
- Crystallographic Information  
(Arrangement of atoms in the specimen; thus direct relation between these arrangements and material properties)
- Cracks and fracture surfaces, bond failures can be analysed with the help of SEM inspection.
- In order to perform compositional analysis on specimens, SEM may be equipped with an EDX (Energy Dispersion Spectroscopy) analysis system
- SEM allows a large amount of sample to be focused at one time. It produces a image that is good representation of the three dimensional sample. Thus SEM inspection has a large depth of field
- SEM is one of the most heavily used instruments in academic lab research areas and industry because of the combination of higher magnification, larger depth of field, greater resolution, compositional and crystallographic information
- SEM application also include roughness measurement, measurement of fractal dimension, examining fracture surface of metals, characterization of materials, corrosion measurement, and dimensional measurements at the nanoscale
- When SEM is combined with chemical analytical capabilities, it not only provides the image of the morphology and microstructures of bulk and nanostructured materials and devices, but can also provide detailed information of chemical composition and distribution.

### 2.2.3 Hall Effect measurements

Electrical characterization of materials evolved in three levels of understanding. In the early 1800s, the resistance  $R$  and conductance  $G$  were treated as measurable physical quantities obtainable from two-terminal  $I$ - $V$  measurements (i.e., current  $I$ , voltage  $V$ ). Later, it became obvious that the resistance alone was not comprehensive enough since different sample shapes gave different resistance values. This led to the understanding (second level) that an intrinsic



material property like resistivity (or conductivity) is required that is not influenced by the particular geometry of the sample. For the first time, this allowed scientists to quantify the current-carrying capability of the material and carry out meaningful comparisons between different samples. Development of quantum mechanics leads to the solution related to the problem of electrical transport. This led to the definitions of carrier density  $n$  and mobility  $\mu$  (third level of understanding) which are capable of dealing with even the most complex electrical measurements today.

The basic principle underlying the Hall Effect is the Lorentz force. When an electron moves along a direction perpendicular to an applied magnetic field, it experiences a force acting normal to both directions and moves in response to this force and the force effected by the internal electric field. The Lorentz force is given by

$$F_{LORENTZ} = q[E + (V \times B)] \dots \dots \dots (2.3)$$

The Hall Effect is illustrated in figure 2.5 for a bar- shaped sample in which charge is carried by electrons. A constant current  $I$  flow through the bar and the entire bar is subject to a uniform magnetic field  $B$ , which is directed in to the screen, perpendicular to the current flow. Since the electrons are travelling through a magnetic field, they are subject to an upwards Lorentz force and so drift to the top of the bar whilst maintaining their horizontal motion. This leads to a buildup of negative charge on one side of the bar and on the other due to lack of electrons. This leads to a potential difference between the two sides of the sample that can be measured as the Hall voltage  $V_H$ .

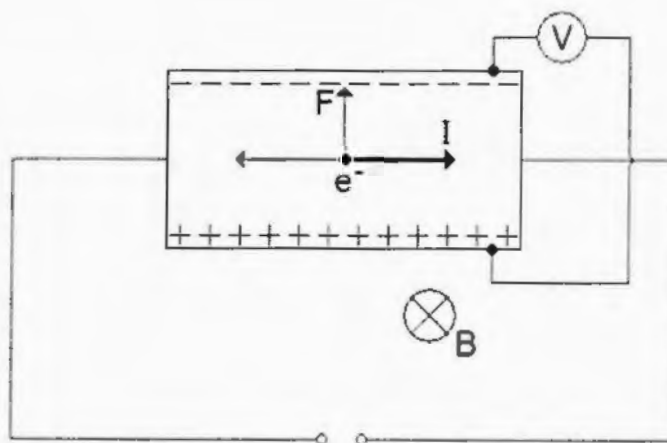


Figure 2.5: Illustration of the Hall Effect in a bar of conducting material.

Hall Effect is also used to determine devices characteristics and performance. Depending on the device in hands we will attain different information. It is a basic electric measurement and a fundamental way to discover behavior and characterize the following devices.

- Semiconductors (ICs, memory, MOS FETs, bipolar transistors, etc.)
- Components (LEDs, sensors, resistors, etc.)
- New materials (Carbon nanotube, Graphene, Nanowire, GMR, organic devices, etc.)
- Other electronic devices (photovoltaic cell, electric circuit, etc.)

There are many parameters which could be extracted from I-V measurements such as threshold voltage and sub threshold slope and resistance.

## 2.2.4 Ultraviolet-Visible (UV-Vis) Spectroscopy

For the last 35 years, Ultraviolet and visible spectrometers have been in general use and in the modern day laboratory it have become the most important analytical instrument over this period. Other techniques could be employed in many applications but none replace UV-Visible spectrometry for its simplicity, versatility, speed, accuracy and cost-effectiveness.

Principle of Ultraviolet-visible (UV-Vis) spectroscopy is that it is used to obtain the absorbance spectra of a compound in solution or as a solid. During this process, actually the absorbance of light energy or electromagnetic radiation is observed spectroscopically. This energy is responsible for the excitation of electrons from the ground state to the first singlet excited state of the compound or material.

For the electromagnetic spectrum the UV-Vis region of energy covers 1.5 - 6.2 eV correspondence to the wavelength range of 800 - 200 nm. Basically we can obtain qualitative and quantitative information of a given compound or molecule from UV-Vis spectroscopic data. A typical UV spectrometer is shown in figure 2.6.

Electromagnetic spectrum consists of Ultraviolet (UV) and visible radiation along with other form of radiation such as radio, infrared (IR), cosmic, and X rays. Energy corresponding with electromagnetic radiation is defined by the following relation:

$$E = h\nu \dots \dots \dots (2.4)$$

Where  $E$  is energy (in joules),  $h$  is Planck's constant ( $6.62 \times 10^{-34} \text{ Js}^{-1}$ ), and  $\nu$  is frequency (in seconds).

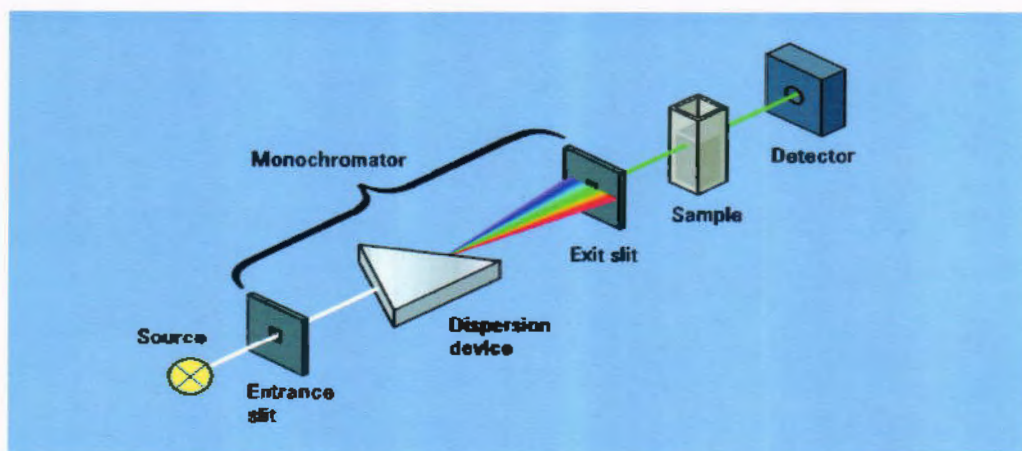


Figure 2.6: Schematic diagram of single beam spectrometer

A number of processes such as including reflection, scattering, absorbance, fluorescence or phosphorescence (absorption and re-emission), and photochemical reaction (absorbance and bond breaking) can occur by the interaction of radiation with matter [27]. An electromagnetic spectrum is illustrated in figure

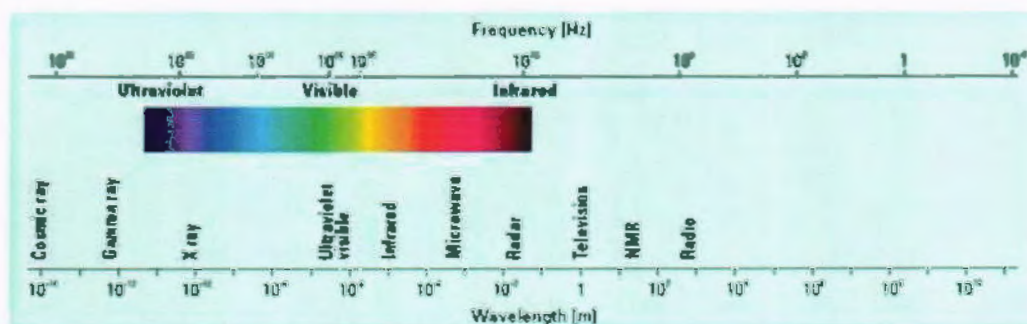


Figure 2.7: Electromagnetic spectrum

Generally, in process of measuring UV-Visible spectra, it is desirable for us that only absorbance occur. Because absorption of light by matter causes the energy content of the molecules (or atoms) to increase. This is due to the fact that light is a form of energy. So generally the total potential energy of molecules represented as the sum of its electronic, vibrational and rotational

$$E_{TOTAL} = E_{Elec} + E_{Vib} + E_{rot} \dots\dots\dots (2.5)$$

We also know that whatever the amount of energy possesses by a molecule, it does not exist in a continuum but instead present in a series of discrete levels or states. Application of UV Vis spectroscopy are as

- UV/Vis spectroscopy is routinely used in analytical chemistry for the quantitative determination of different analyses, such as transition metal ions, highly conjugated organic compounds, and biological macromolecules. Spectroscopic analysis is commonly carried out in solutions but solids and gases may also be studied.
- Solutions of transition metal ions can be colored (i.e., absorb visible light) due to the d electrons within the metal atoms can be excited from one electronic state to another. The colour of metal ion solutions is strongly affected by the presence of other species, such as certain anions or ligands.
- Organic compounds, especially those with a high degree of conjugation, also absorb light in the UV or visible regions of the electromagnetic spectrum. The solvents for these determinations are often water for water-soluble compounds, or ethanol for organic-soluble compounds. (Organic solvents may have significant UV absorption; not all solvents are suitable for use in UV spectroscopy. Ethanol absorbs very weakly at most wavelengths.) Solvent polarity and pH can affect the absorption spectrum of an organic compound.
- While charge transfer complexes also give rise to colors, the colors are often too intense to be used for quantitative measurement.
- UV-Vis spectroscopy is also used in the semiconductor industry to measure the thickness and optical properties of thin films on a wafer
- UV-Vis spectrometers are used to measure the reflectance of light, the Index of Refraction (n) and the Extinction Coefficient (k) of a given film across the measured spectral range
- The Beer-Lambert law states that the absorbance of a solution is directly proportional to the concentration of the absorbing species in the solution and the path length. Thus, for a fixed path length, UV/Vis spectroscopy can be used to determine the concentration of the absorber in a solution

Transmittance and concentration according to Beer's law is illustrated in figure 2.8

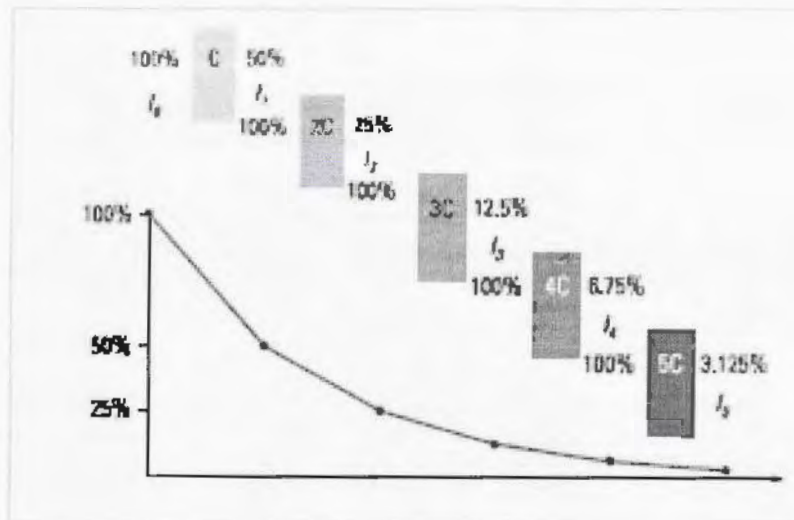


Figure 2.8: Graph of transmittance and concentration (Beer's law)

The difference between Beer's law and Bouguer's law (Beer-Bouguer-Lambert law) is that it is stated in terms of concentration. The amount of light absorbed in UV Vis spectroscopy is proportional to the number of absorbing molecules through which the light passes. Figure 2.8 also shows a plot of transmittance against path length. Mathematical form of Beer-Bouguer-Lambert law can be written as follows:

$$T = \frac{I}{I_0} = e^{-kbc} \dots \dots \dots (2.6)$$

In this equation "c" is the concentration of the absorbing species (usually expressed in grams per liter or milligrams per liter). Now by taking the logarithm of above equation, it can be transformed into a linear expression expressed as

$$A = \log T = \log \left( \frac{I}{I_0} \right) = \epsilon bc \dots \dots \dots (2.7)$$

Where  $\epsilon$  in above equation is the molar absorption or extinction coefficient. This expression is commonly known as Beer's law.

### 2.2.4 Ellipsometry

Ellipsometry measures a change in polarization as light reflects or transmits from material structures. The polarization change is represented as an amplitude ratio,  $\Psi$ , and the phase difference,  $\Delta$ . The measured response depends on optical properties and thickness of individual materials. Thus, ellipsometry is primarily used to determine film thickness and optical

constants. However, it is also applied to characterize composition, crystallinity, roughness, doping concentration, and other material properties associated with a change in optical response.

Since 1960s, as ellipsometry developed to provide the sensitivity necessary to measure nanometer scale layers used in microelectronics, interest ellipsometry has grown steadily [28]. Today, the range of its applications has spread to the basic research in physical sciences, semiconductor and data storage solutions, flat panel display, communication, biosensor, and optical coating industries. This widespread use is explained by increased dependence on thin films in many areas and the flexibility of ellipsometry to measure most material types: dielectrics, semiconductors, metals, superconductors, organics, biological coatings, and composites of materials.

In ellipsometry, an electromagnetic radiation is emitted by a light source and linearly polarized by a polarizer. It can pass through an optional compensator (retarder, quarter wave plate) and falls onto the sample. After reflection the radiation passes a compensator (optional) and a second polarizer, which is called an analyzer, and falls into the detector. Instead of the compensators, some ellipsometers use a phase-modulator in the path of the incident light beam. A schematic figure of scanning electron microscope is illustrated in figure 2.9.

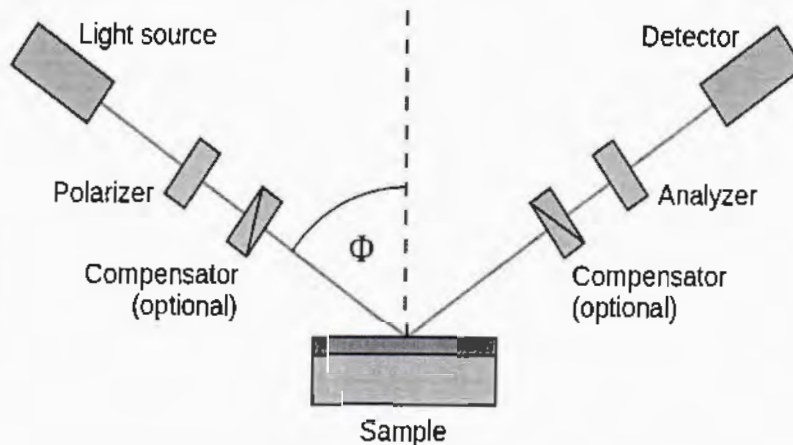


Figure 2.9: Schematic diagram of ellipsometry experiment

Ellipsometry is a specular optical technique (the angle of incidence equals the angle of reflection). The incident and the reflected beam span the plane of incidence. Light which is polarized parallel to this plane is named p-polarized (p-polarised). A polarization direction

perpendicular is called s-polarized (s-polarised), accordingly [29]. Ellipsometry has a number of advantages compared to standard reflection intensity measurements:

- Ellipsometry measures at least two parameters at each wavelength of the spectrum. If generalized ellipsometry is applied up to 16 parameters can be measured at each wavelength.
- Ellipsometry measures an intensity ratio instead of pure intensities. Therefore, ellipsometry is less affected by intensity instabilities of the light source or atmospheric absorption.
- By using polarized light, normal ambient unpolarized stray light does not significantly influence the measurement, no dark box is necessary.
- No reference measurement is necessary.
- Both real and imaginary part of the dielectric function (or complex refractive index) can be extracted without the necessity to perform a Kramers–Kronig analysis.
- Ellipsometry is especially superior to reflectivity measurements when studying anisotropic samples.

TH17283

## Chapter 3 Results & Discussions

In chapter 3, we will discuss in detail the results to analyze the structural, optical and electrical properties of ZnS thin films prepared with different growth parameters and doping materials. Results of our prepared films related with their structural, optical, electrical and morphological analysis are as follows.

### 3.1 Structural analysis

In order to investigate the crystal structure of the film, XRD measurements were performed. The D8 Discover HR-XRD is used for XRD measurements. Using these XRD results we investigate the effect of deposition temperature, deposition time along with doping on the structural properties of thin films.

#### 3.1.1 Effect of temperature

Figures 3.1 show XRD results related to ZnS thin films grown by chemical bath deposition at two different temperatures i.e 32°C and 84°C

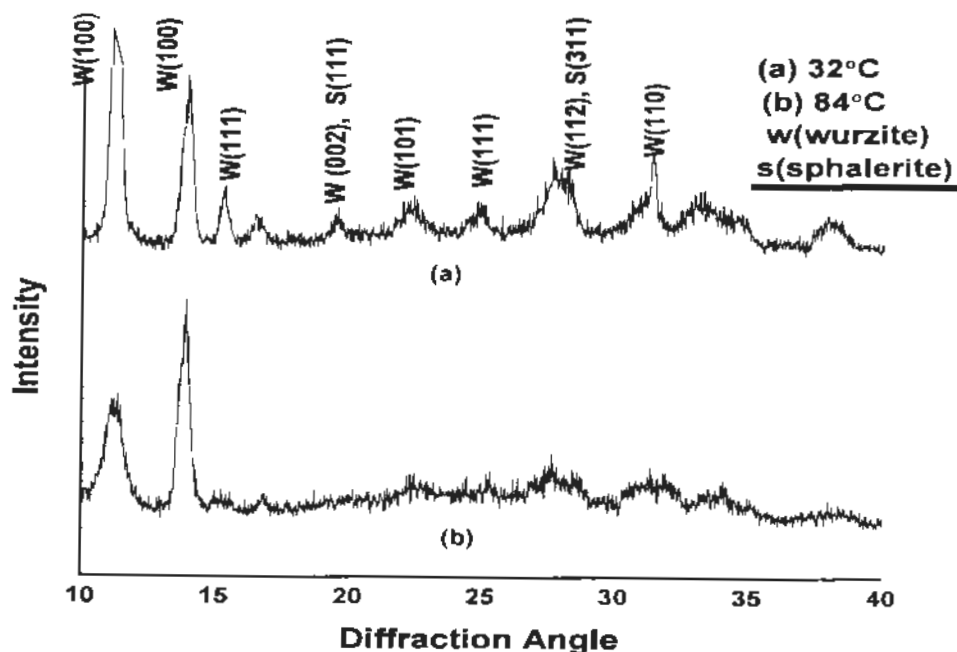


Figure 3.1: XRD pattern of ZnS films deposited at different temperature (a)  $T=32^{\circ}\text{C}$   
(b)  $T=84^{\circ}\text{C}$



From above XRD pattern we can concluded that the crystallinity of ZnS thin films increases with the increase in temperature. In figure 3.1(a) peak (111) and (110) corresponding to cubic structure of ZnS thin films whereas peaks in figure 3.1(b) also shows the formation of crystal structure of wurtzite and sphalerite (zinc blende) in ZnS thin film (JCPDS card no 77-2100). Taisuke Iwashita et al. have achieved the similar kind of XRD results for ZnS films grown through chemical bath deposition method [30].

Grain size is calculated by using the Debye scherrer formula

$$D = K\lambda / \beta \cos\theta \dots \dots \dots (3.1)$$

Where  $\lambda$  is the wavelength of X-rays,  $\beta$  is the angular line width at half maximum in radians and  $\theta$  is the Bragg diffraction angle. The micro-strain can be calculated by using the formula [31]

$$\epsilon = \beta \cos\theta / 4 \dots \dots \dots (3.2)$$

Other parameter such as d-spacing was also calculated by using equation 2.2. Our corresponding results were as follows

*Table 3.1: Structural Parameters of ZnS films calculated through XRD measurement*

Samples	Grain Size(nm)	d-Spacing( $\text{\AA}$ )	Lattice strain ( $\epsilon$ )
ZnS (32 $^{\circ}$ C)	2.01	0.79	0.101
ZnS (84 $^{\circ}$ C)	3.48	1.09	0.134

Similar kind of results for d-spacing were also achieved for ZnS films grown by chemical bath deposition by Qi Liu et al. [32].

### 3.1.2 Effect of deposition time

As we have seen in pervious section that the films deposited at 84 $^{\circ}$ C had better structural quality so we have tried to optimize the film quality by changing the time of deposition by keeping temperature of bath at 84 $^{\circ}$ C. Figures 3.2 show XRD pattern of ZnS thin films deposited for three different deposition time i.e., 1.5 hr., 2 hr. and 2.5 hr. at fixed temperature of 84 $^{\circ}$ C. We observed more peaks as the deposition time increases, so we can assume that the crystallinity of films got better. From these graph, some other diffraction peak were observed at  $2\theta = 10-$

40°, some of these corresponds to glass, which is amorphous in nature, which is also consistent with the literature [33]. Peak (100), (111), (002), corresponds to cubical structure of ZnS. This diffraction pattern confirmed the cubical structure of ZnS (JCPDS card no. 72-0613). Grain size varies from 2.7nm to 3.9nm corresponding to peaks (110) and (111) respectively. Similarly d- spacing and lattice constant calculated by using equations (2.2) & (3.2) remains the same as discussed in section 3.1.1.

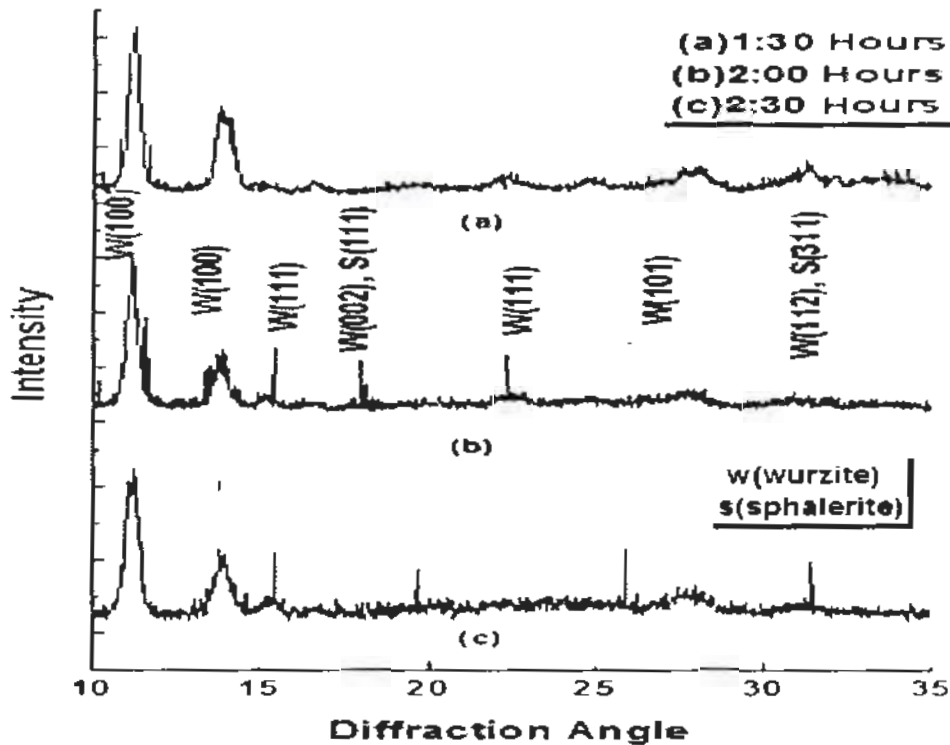


Figure 3.2: XRD pattern of ZnS films deposited at different deposition time (84°C)

### 3.1.3 Effect of Doping in ZnS films

XRD pattern for Cu and Fe doped of ZnS thin films are shown in figure 3.3 & 3.4. There are no distinct peaks were observed in both pattern showing the amorphous nature of thin films. Few diffraction peaks corresponding to (111), (220) and (311) planes show cubical structure of undoped ZnS (Zinc blende JCPDS 050566). Similar kind of results for doped samples of ZnS films have achieved [34, 35]. Grain size found to increase due to the doping of Cu and Fe in ZnS thin films. Other parameters include lattice constant, d-spacing were also calculated. Our corresponding results were as follows

Table 3.2: Structural Parameters of doped ZnS calculated from XRD measurements

Samples	Grain size(nm)	Lattice strain ( $\epsilon$ )	d-spacing value(nm)
Cu doped ZnS	4.6	3.353	6.93
Fe doped ZnS	13.2	7.109	3.53

These values were also calculated from the data using equations (3.1), (3.2) & (2.2). The change in lattice parameters could be well understood by the substitution of  $\text{Cu}^{2+}$  ions (ionic radius =  $0.73 \text{ \AA}$ ) which is larger than that of  $\text{Zn}^{2+}$  ions (ionic radius =  $0.74 \text{ \AA}$ ) [36]. Similarly it is well known that ionic radius of  $\text{Fe}^{2+}$  ( $0.77 \text{ \AA}$ ) is close to that  $\text{Zn}^{2+}$ , and therefore it is reasonable to speculate that it is easy for  $\text{Fe}^{2+}$  to penetrate into ZnS lattice or to substitute the  $\text{Zn}^{2+}$ . Figure 3.3 and 3.4 shows the XRD pattern corresponding to Fe and Cu respectively.

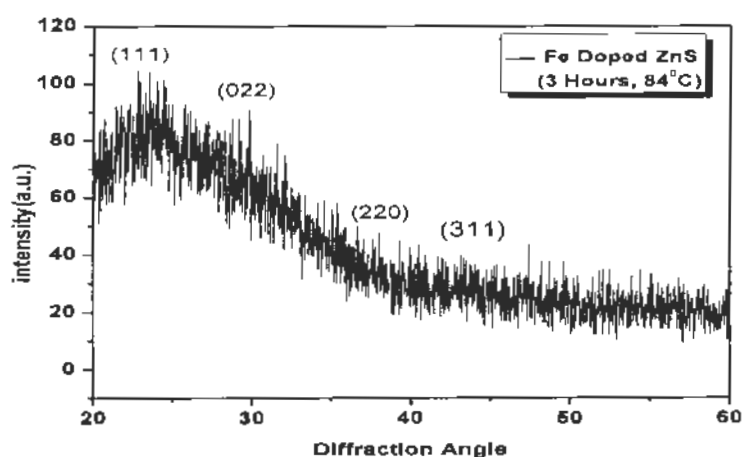


Figure 3.3: XRD pattern of Fe doped ZnS thin film

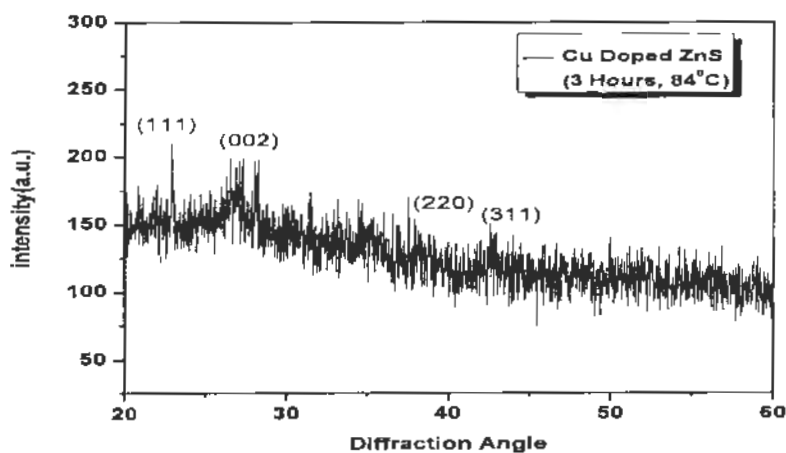


Figure 3.4: XRD pattern of Cu doped ZnS thin film

Oladeji and Chow reported that chemically deposited ZnS thin films are highly disorder materials [9], which is also confirmed by highly amorphous behavior depicted through our XRD pattern.

### 3.2 Morphological Studies

SEM images have been obtained for each of the grown film, in order to investigate the micro-structural surface topography. Figures represent SEM micrographs of the surface of the samples prepared by CBD. We shall discuss the effect of all the parameters changed during growth on the surface properties.

#### 3.2.1 Effect of temperature

SEM images for ZnS samples at two different temperatures such as 32°C and 84°C are shown in fig 3.5 (a) and (b) respectively.

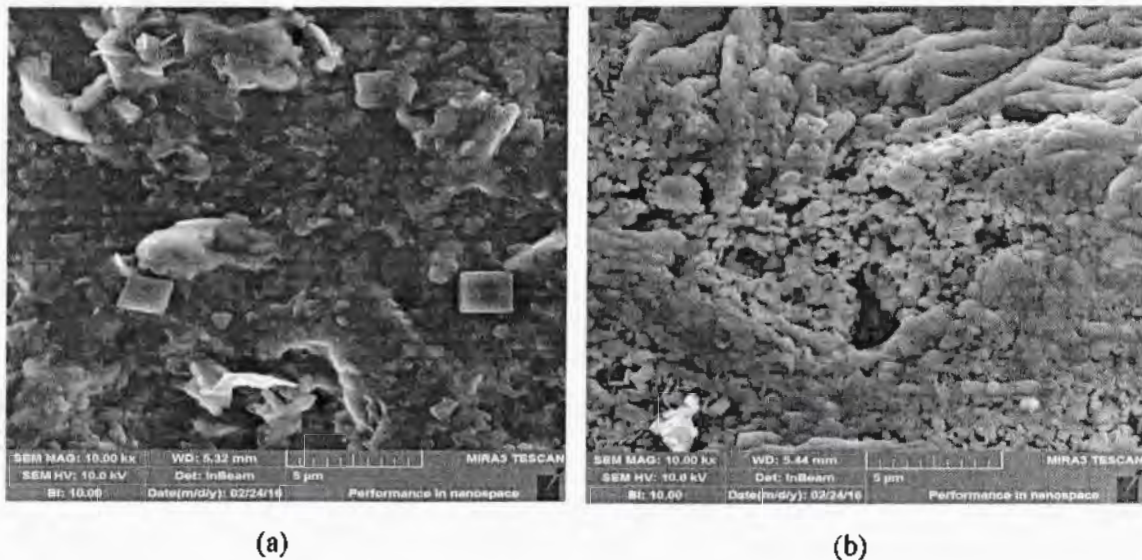


Figure 3.5: SEM micrographs for ZnS film deposited at different temperature (a) 32°C (3hrs) (b) 84°C (3 hrs.)

SEM images shows the surface morphology of samples at two different temperatures such as 32°C (room temperature) and 84°C (higher temperature). It can be seen that morphology of the surface become dense and granular structure increased with the increased in the temperature. Same kind of results were also achieved by Limei Zhou et al. [37]. Particles size has also

increased with increasing temperature. EDX results in figure 3.6, also confirms the formation of ZnS thin films. Atomic percentage is as follows

*Table 3.3: Atomic percentage in ZnS film*

Element	Weight %	Atomic %
N K	14.03	29.99
O K	13.47	25.22
Si K	0.90	0.96
S K	23.15	21.62
Zn K	48.46	22.20

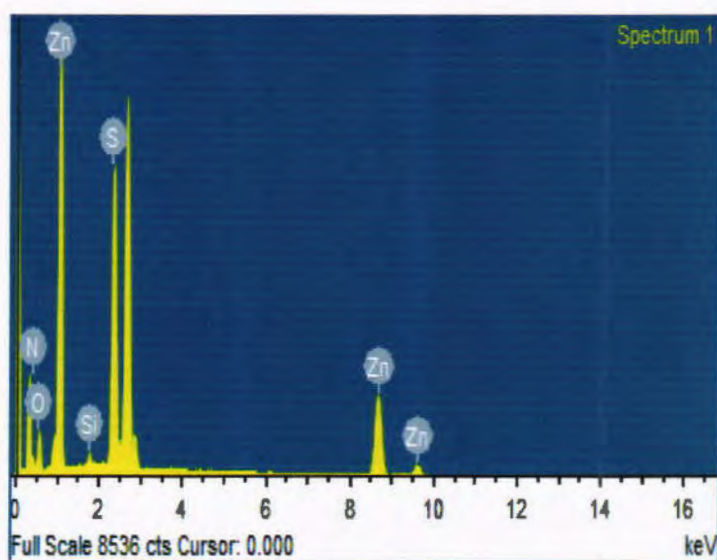
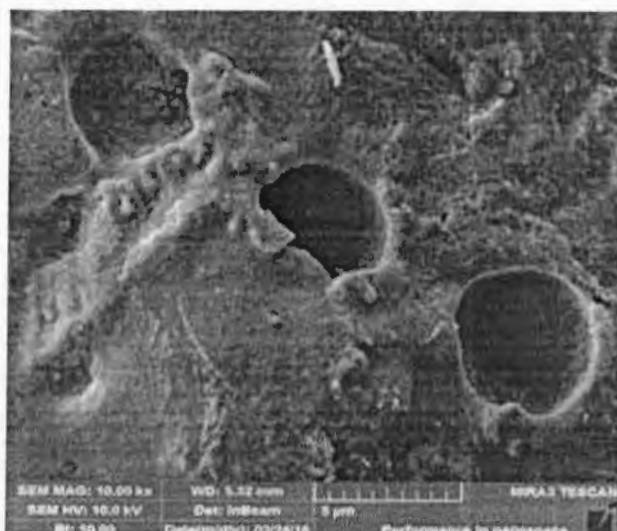


*Figure 3.6: EDX result of ZnS film*

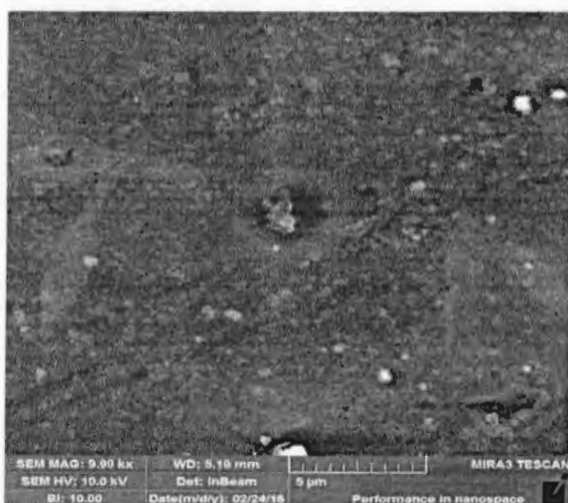
From EDX results we observed that in our prepared samples nitrogen, oxygen and silica are also present. Basically all of these are the impurities. The presence of these impurities are mainly due to drying of samples in open atmosphere. Nitrogen is also present in the vacuum chamber of SEM machine. Silica is also present, which is due to glass substrate.

### 3.2.2 Effect of deposition time

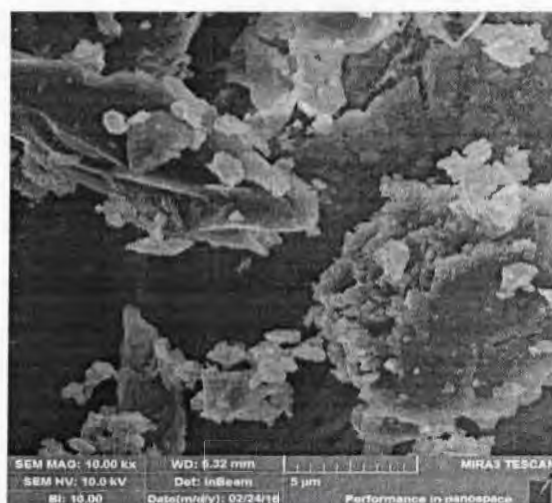
SEM micrographs for different deposition time such as 1.5, 2.0, 2.30 hours are shown in figure 3.7 (a), (b) and (c) respectively.



(a)



(b)



(c)

*Figure 3.7: SEM micrographs for ZnS film deposited at different deposited at different deposition time (a) 1:30 hrs. (b) 2:00 hrs. (c)2:30 hrs.*

ZnS films deposited at different deposition time such as 1:30 hrs, 2:00 hrs, 2:30 hours. Film in figure 3.7 (b) shows smooth structure but as the deposition time increases, several small particles were present on the surface. Particle size enlarged with increasing deposition time. Increase in grain size with the increase in deposition temperature is also reported by Limei

Zhou et al. [38]. Similarly the surface structure becomes more granular and dense with the increasing deposition time.

Thus it can be concluded that longer deposition time will allow more time for ZnS nuclei to settle on the film surface and because of this our film in figure 3.5 appears more dense.

### 3.2.3 Effect of doping

In the case of doping of ZnS films with Cu and Fe, our SEM images are shown in figures 3.8.

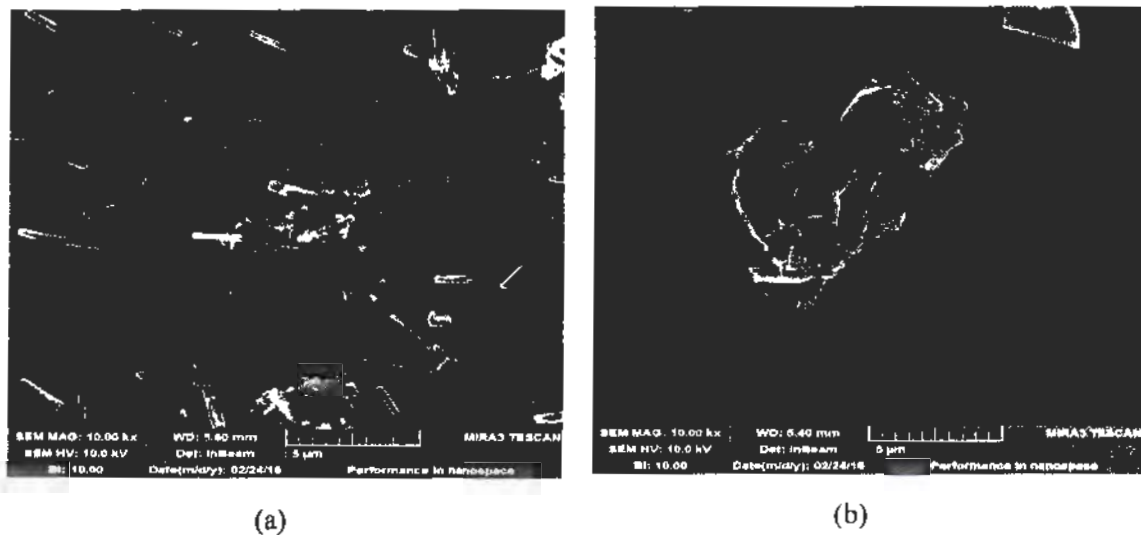


Figure 3.8: SEM micrographs for doped ZnS film (a) Cu doped ZnS (b) Fe doped ZnS

Small aggregates with elongated shape are observed in SEM image of Cu doped ZnS film. These structures are due to anisotropic collection within the solution because of the formation of both ZnS and CuS particles, which is consistent with the results reported in the literature [39]. Similarly, in the case of Fe-doped ZnS film, we also observed a nano-crystalline structure in the form of rods and spherical clusters. Thus overall we conclude that with doping of ZnS films with Cu and Fe, we observed a change in morphology from granular structure to a tube-like structure.

## 3.3 Electrical properties

In order to investigate electrical properties, we used research-grade Hall measurement. Electrical properties are measured using a Nano-chip reliability grade Hall effect system. I-V curves related to our samples are as shown in figure 3.9 and 3.10.

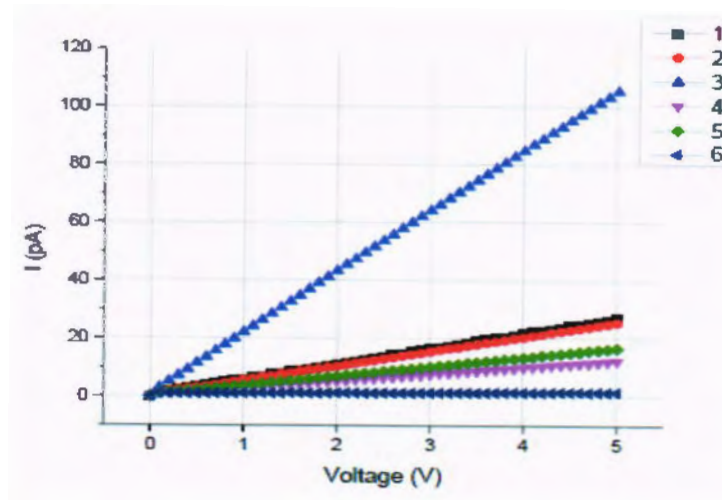


Figure 3.9: I-V curves of samples (1) ZnS at 84°C (1:30 Hours) (2) Cu doped ZnS (3) ZnS at 32°C (3 Hours) (4) ZnS at 84°C (2:30 Hours) (5) ZnS at 84°C (2 Hours) (6) ZnS at 84°C (3 Hours)

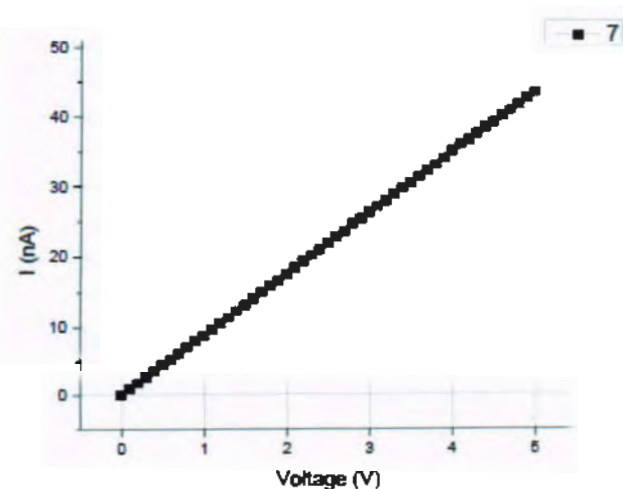


Figure 3.10: I-V Curves of sample (7) Fe Doped ZnS

Figures show the I-V curves of doped and undoped samples of ZnS. In all these figures it had been observed that current and voltage shows linear behavior. So ZnS film does not have semi conductivity properties as we have not used the dopants suitable to enhance the electrical conductivity. It is clear from the figures that all the films are highly resistive as the current measured has very low values, might be corresponding to or comparable to the system noise.

I-V curve of ZnS thin film grown at room temperature shows slightly higher values of current. Still the values are lying in pA range. I-V characterization for Fe doped ZnS thin film is



presented in figure 3.10. Current levels are higher than other films but still not corresponding to semiconducting regime.

Other parameters such as carrier concentration, conductivity, sheet carrier mobility are so small that they were out of range to measure. Overall we can say that electrical properties of chemically deposited ZnS films are not up to mark for device design. We can improve their quality in future by changing the dopant appropriate to electrical characteristics.

### 3.4 Optical properties through UV-Vis Spectroscopy

Optical properties of the thin films deposited on glass substrate are determined by using UV-Vis spectrometer. Details of the measurements and then step by step analysis are given in coming section

#### 3.4.1 Transmittance

Using Hitachi UV-VIS spectrometer the transmittance spectrum of all thin films was measured. The transmittance is “Ratio of the transmitted intensity to the incident intensity of the radiation” Using appropriate equations absorbance, reflectance, along with other optical properties were calculated from the transmittance values. Figures 3.11-3.13 shows the transmission spectrum of different samples.

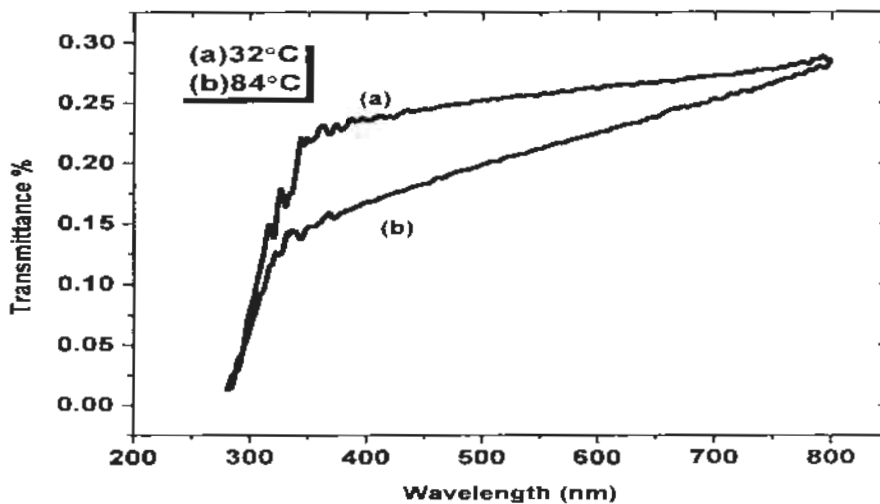


Figure 3.11: Transmission graph of ZnS deposited at different temperature (3hrs.)

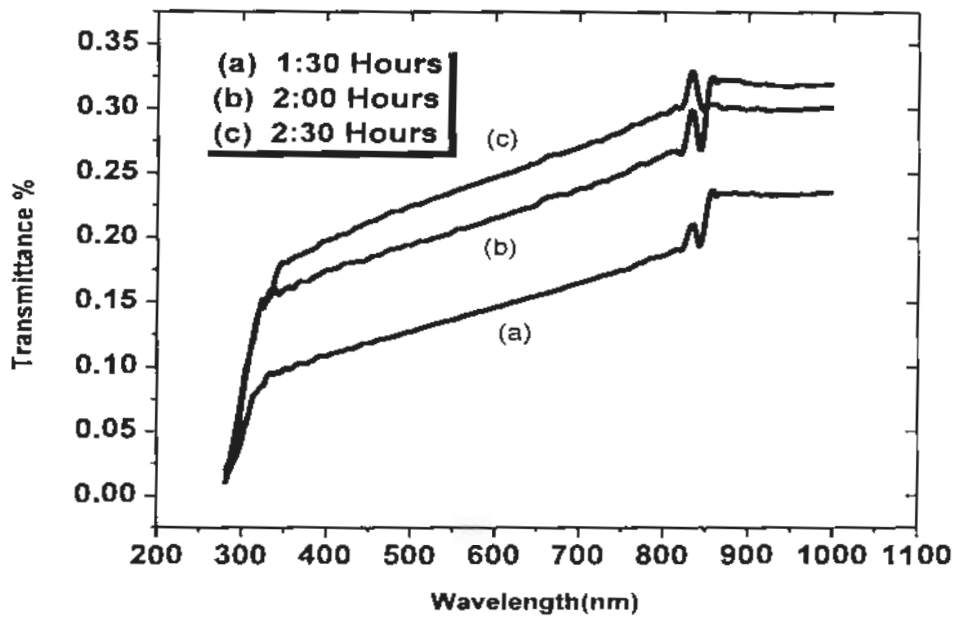


Figure 3.12: Transmission Graph for ZnS deposited for different deposition time (84°C)

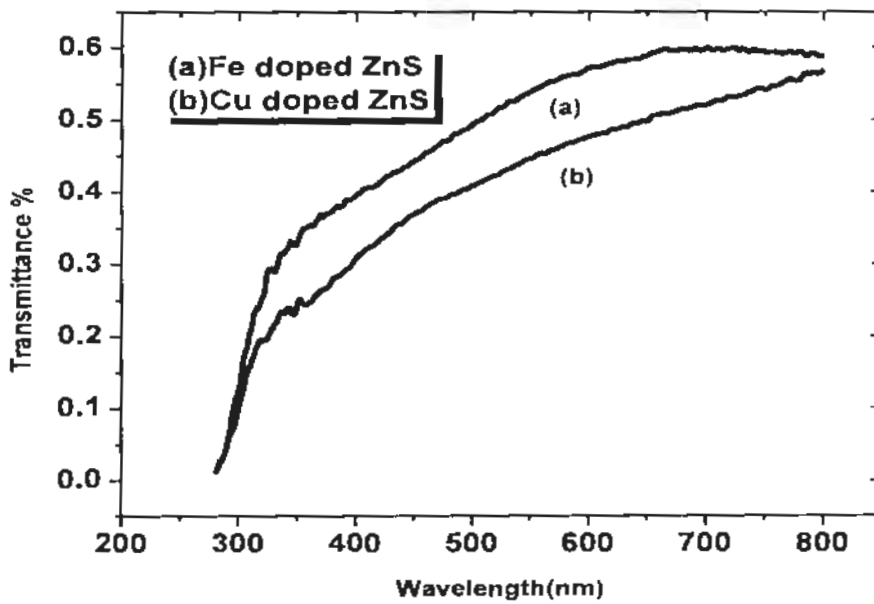


Figure 3.13: Transmission graph for doped ZnS films with Cu and Fe

All the samples are semitransparent in nature therefore transmission of our samples, mostly present in visible region (52%-68%). Qi Liu et.al have achieved the similar kind of results for ZnS films grown through chemical bath deposition method [32, 40]. Whereas in the case of doped samples transmittance value enhanced from almost 0.1% to 0.6%. Thus we can conclude from these results that our prepared doped samples of ZnS shows high transmittance so probably it can be used as buffer layer in solar cell. Similarly from figures 3.11-3.13 it is observed that our samples had a very low transmission in UV region, thus we can conclude that it can be used as UV shield as depicted by transmittance graphs.

### 3.4.2 Absorbance

Absorption is the process in which the energy of a photon is absorbed through electronic transition in inter-band or intra-band regime. The absorbance was calculated using transmittance value through following equation 2.7.

$$A = \log_{10} \left\{ \frac{1}{T} \right\} \dots \dots \dots (3.3)$$

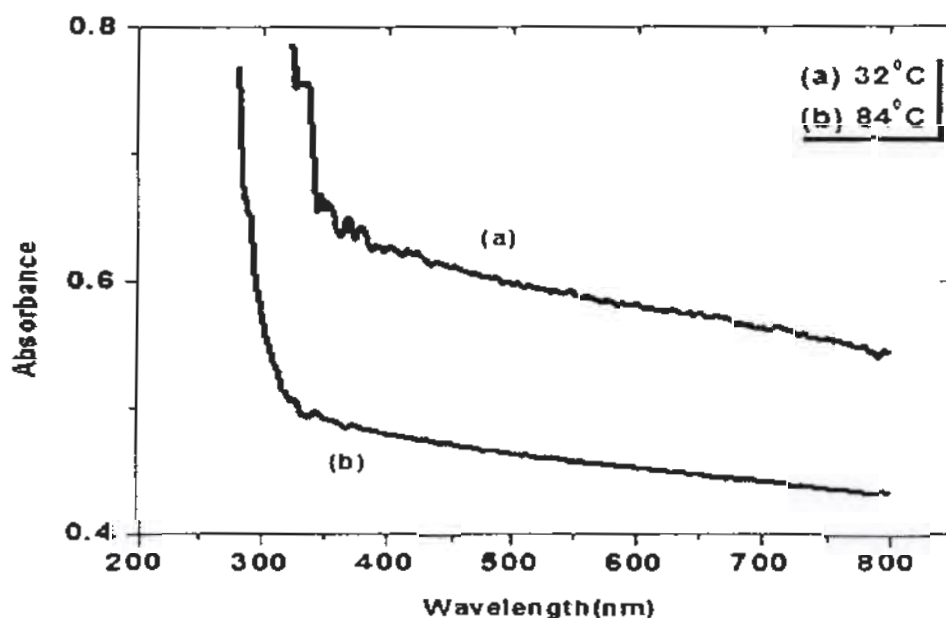


Figure 3.14: Absorbance graph for ZnS deposited at different temperature (3hrs)

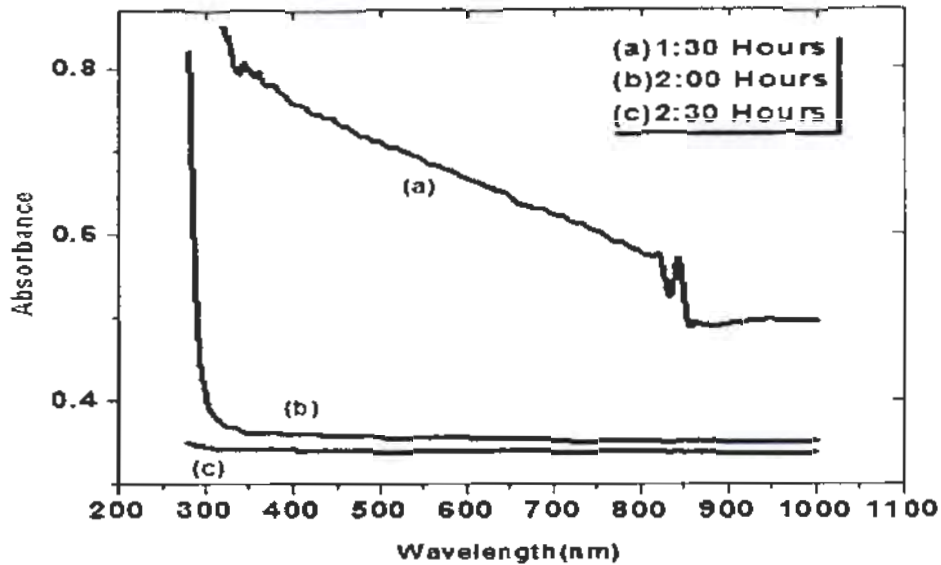


Figure 3.15: Absorbance graph for ZnS deposited at different deposition time (84°C)

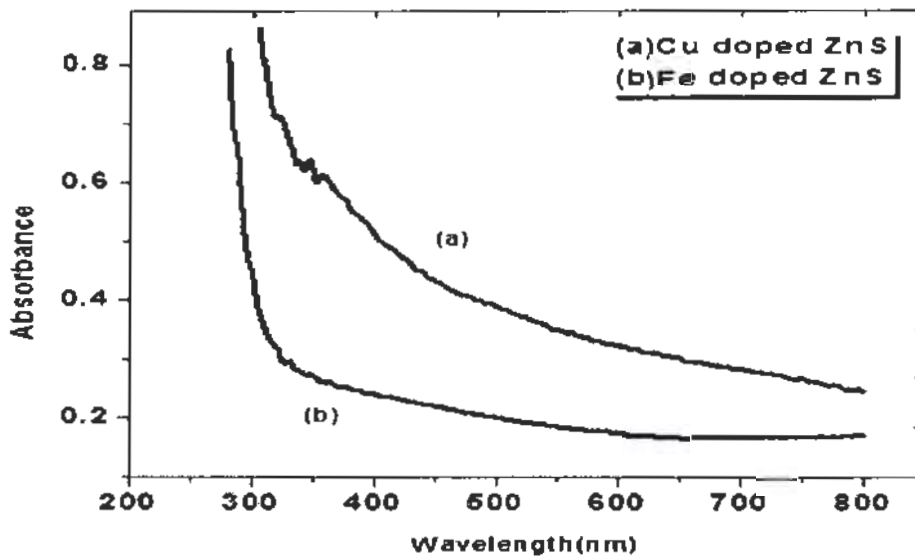


Figure 3.16: Absorbance graph for doped ZnS with Cu and Fe

A sharp decrease in absorbance is observed in the UV portion for all samples. If we compared results of all these films, we observe that this decrease is sharp in ZnS films as compared with the doped one. This observed abrupt increase in absorption is due to the UV cut-off of the used glass substrate. Thus doped ZnS samples can be made good UV absorber and also in UV industry can be used as UV sensor.

### 3.4.3 Reflectance

Ratio of the reflected to the incident intensity is known as reflectance. It was calculated using relation as

$$R = 1 - (T + A) \dots \dots \dots (3.4)$$

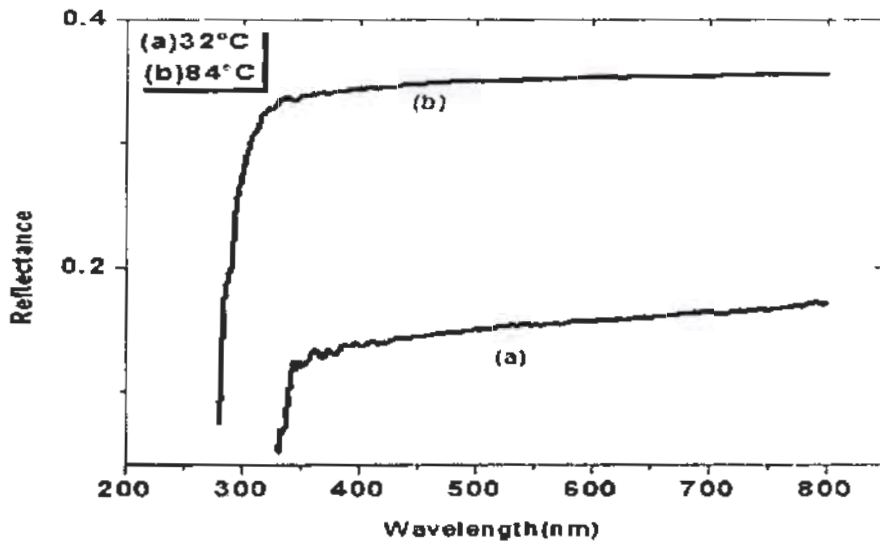


Figure 3.17: Reflectance graph of ZnS deposited at different temperature (3 hrs.)

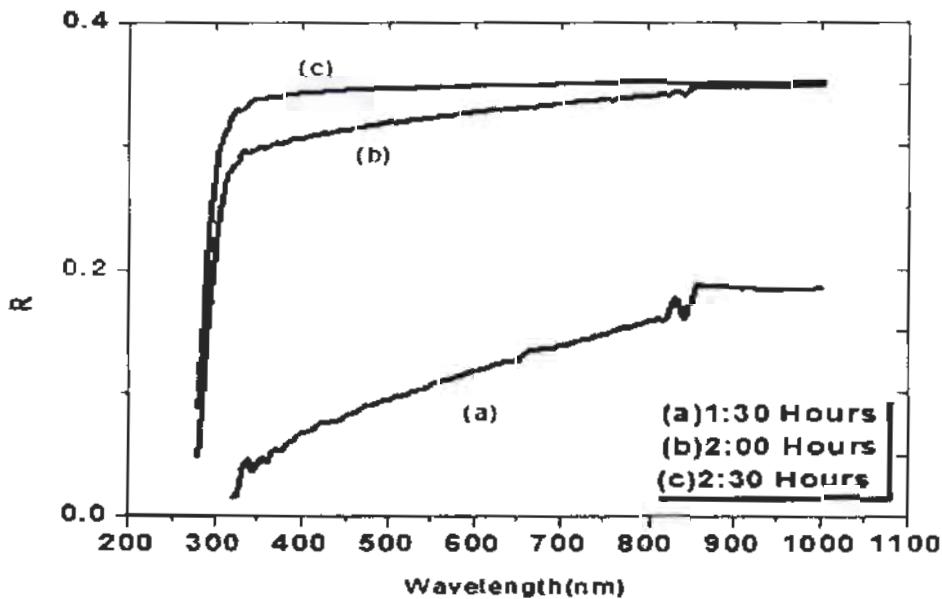


Figure 3.18: Reflectance graph of ZnS deposited at different deposition time (84°C)

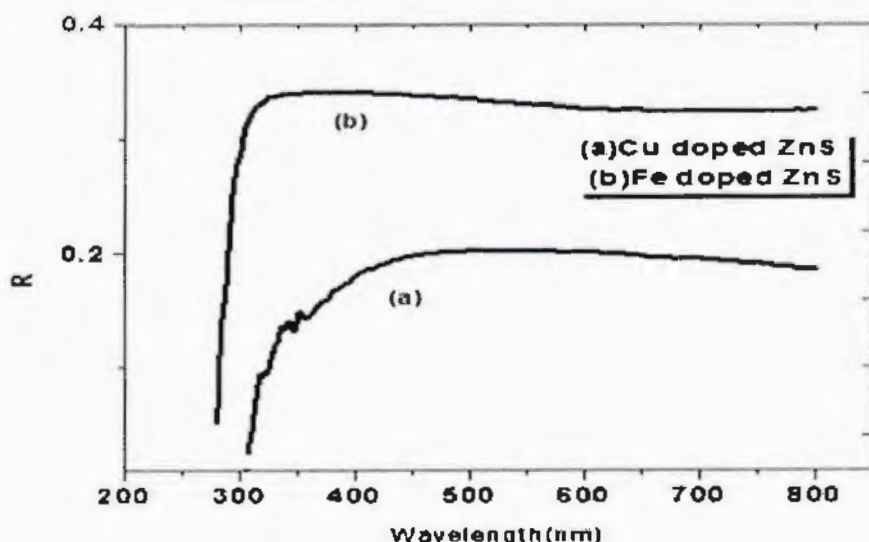


Figure 3.19: Reflectance graph of doped ZnS with Cu and Fe

From figures 3.17-3.19 we observed that in all samples reflectance is increasing with increasing wavelength. This may be due to the films thickness and roughness, which is varying in all film. It can be seen that the deposited film for smaller time has higher transparency, because it was thinner than the others. Moreover, this film was not densely covered by particles and the space of particles was large so the light can transmit easily. In general reflectance is increasing. It can therefore be used in multi-layer thin film devices. Films with high reflectance is used to form coatings on dielectric materials and others, typically for solar energy collectors.

### 3.4.4 Absorption coefficient

Attenuation per unit thickness of the film is absorption coefficient. With the wavelength of impinging electromagnetic radiation, absorption coefficient change. It is related to transmittance through following relation [41]

$$\alpha = \frac{\{\ln[1/T]\}}{x} \dots \dots \dots (3.5)$$

In this equation x is thickness of the films. Which can be calculated by using the following relation [42, 43]

$$X = \frac{1}{4n} \left[ \frac{\lambda_M \lambda_m}{\lambda_M - \lambda_m} \right] \dots \dots \dots (3.6)$$

In this equation  $\lambda_M$  and  $\lambda_m$  are the wavelengths corresponding to maximum and minimum transmission. The calculated thickness of our prepared films is shown in table 3.4.

*Table 3.4: Comparison of thickness of ZnS films calculated by UV-Vis transmission & ellipsometry*

Samples	Thickness (nm) from UV Vis data	Thickness(nm) from ellipsometry
32°C (3:00 Hours)	29.34	27.13
84°C (3:00 Hours)	33.17	27.16
84°C (1:30 Hours)	29.87	26.77
84°C (2:00 Hours)	30.15	28.04
84°C (2:30 Hours)	32.56	29.05

The calculated thickness in the case of doping with Cu and Fe are shown in table 3.5.

*Table 3.5: Comparison of thickness of doped ZnS films calculated by UV-Vis transmission & ellipsometry*

Samples	Thickness (nm) from UV Vis data	Thickness(nm) from ellipsometry
Cu doped Zns	32.5	29.15
Fe doped ZnS	28.54	24.31

Absorption coefficient calculated through equation (3.5) as a function of wavelength for all thin films are plotted in figure 3.20 to figure 3.22. Figures show that absorption coefficient of all samples. It was observed that value of absorption coefficient decreased corresponding to the wavelength of almost 340nm. Which is consistent with the result achieved by Onwuemeka et al. [40]. However it can also observed that with increasing deposition time, somehow an increasing in extinction coefficient can also be observed in ZnS films from wavelength 400nm to 900 nm respectively. This behavior of increasing is due to the less adhesivity of ZnS on glass substrate.

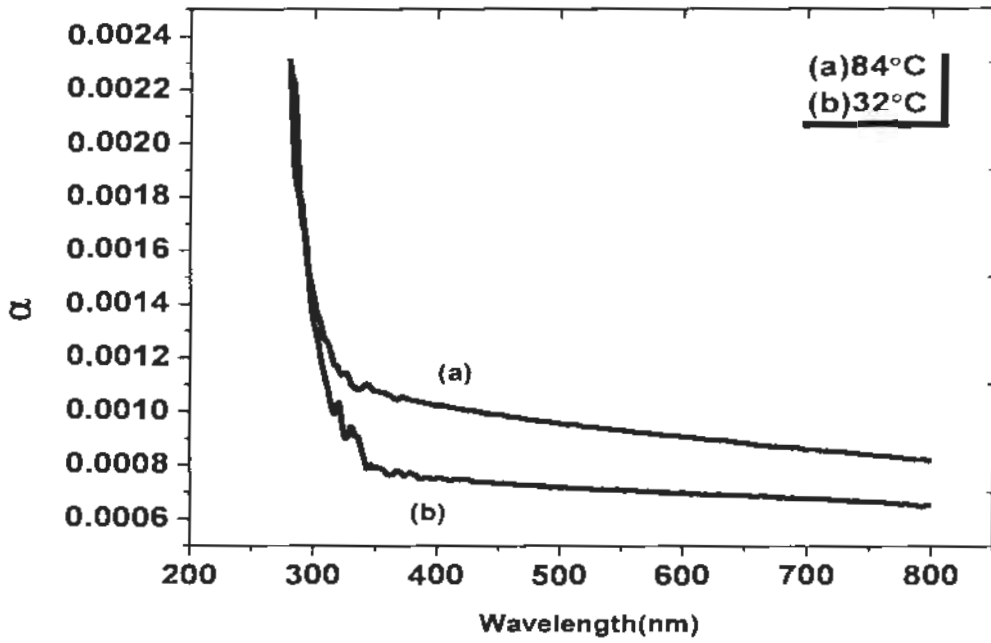


Figure 3.20: Absorption coefficient graph of ZnS deposited at different temperature (3hrs)

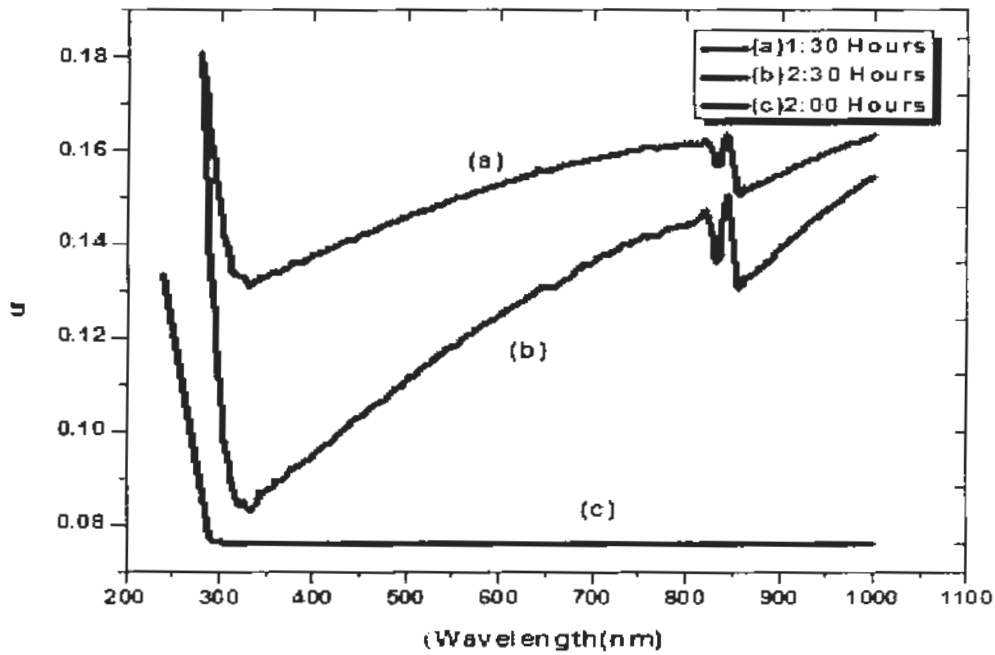


Figure 3.21: Absorption coefficient graph of ZnS deposited at different deposition time (84°C)



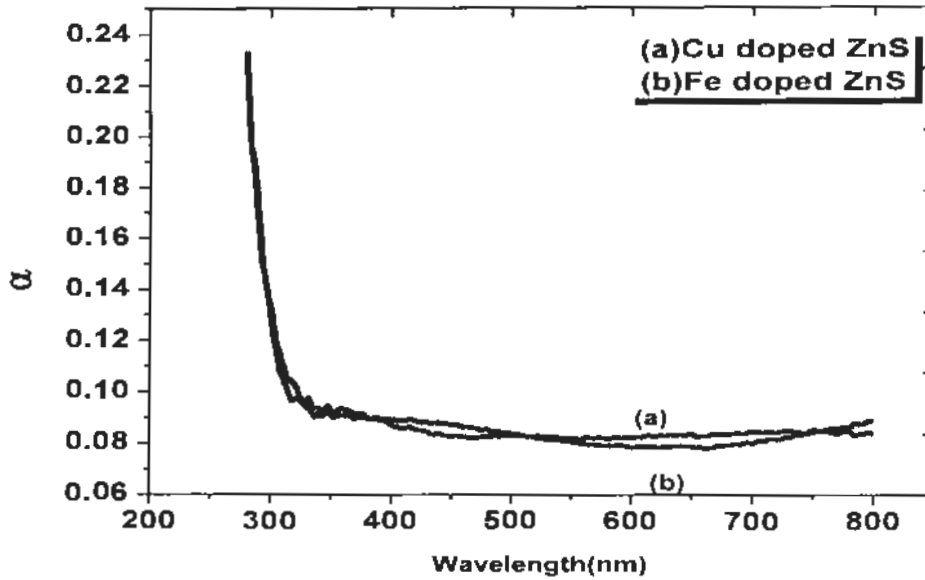


Figure 3.22: Absorption coefficient graph for doped ZnS with Cu and Fe

### 3.4.5 Energy band gap

We calculated the band gap of films from UV Vis spectrum data by using tauc plot. Based on the obtained optical transmission measurements, the square of absorption coefficient  $(\alpha h\nu)^2$  is plotted as a function of photon energy  $(h\nu)$  in figures 3.23-3.25. As it can be seen,  $(\alpha h\nu)^2$  vary almost linearly with  $h\nu$  above the band gap energy ( $E_g$ ). Accordingly, the following equation for direct inter-band transition can be applied [44]

$$(\alpha h\nu)^2 = A(h\nu - E_g) \dots \dots \dots (3.7)$$

Where A is constant. The band gap is obtained by extrapolating the linear portion of the plots to intercept the  $h\nu$  axis. The band gap energy values of ZnS films grown at different temperature are shown in table 3.6.

Table 3.6: Band gap values of ZnS Films from UV-Vis transmission

Samples	Calculated Band gap eV
ZnS at 32°C (3 Hours)	3.75
ZnS at 84°C (3 Hours)	3.6

Our doped samples of ZnS with Cu and Fe show an increase in band gap of 3.8 eV to 3.9 eV respectively. This band gap were also achieved by Daniela et al for Cu doped thin films of ZnS grown by chemical bath deposition method [39]. This shift in band gap values after doping metal is due to the creation of defects levels in the film, which may change the electronics structure of the material.

### 3.4.6 Refractive index

The refractive index is given by equation [40]

$$n = \frac{\{1 + (R)^{1/2}\}}{\{1 - (R)^{1/2}\}} \dots \dots \dots (3.7)$$

Plot of refractive index vs wavelength for undoped and doped ZnS films deposited by chemical bath deposition are shown in Figures 3.26-3.28.

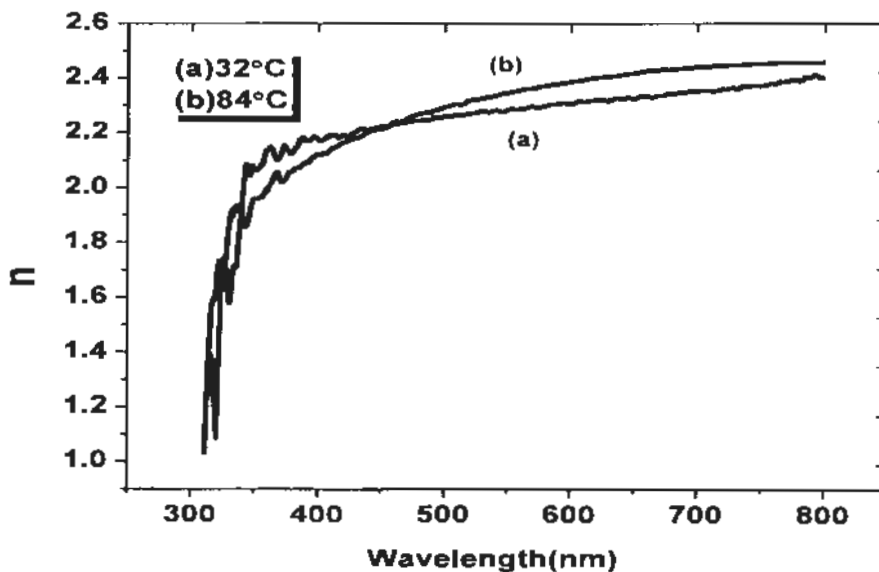


Figure 3.26: Plot of refractive index vs wavelength  $\lambda$  for ZnS films deposited at different temperature (3 hrs.)

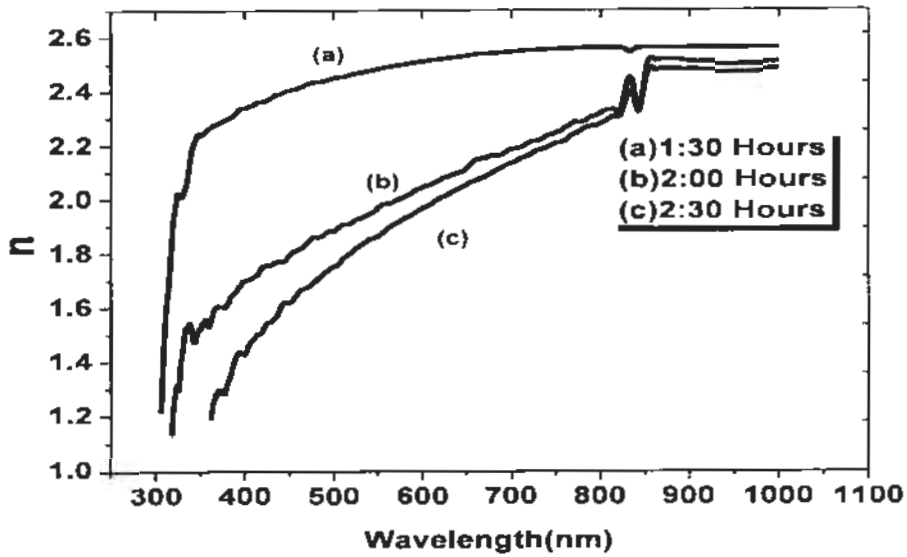


Figure 3.27: Plot of refractive index vs wavelength  $\lambda$  for ZnS films deposited at different deposition time (84°C)

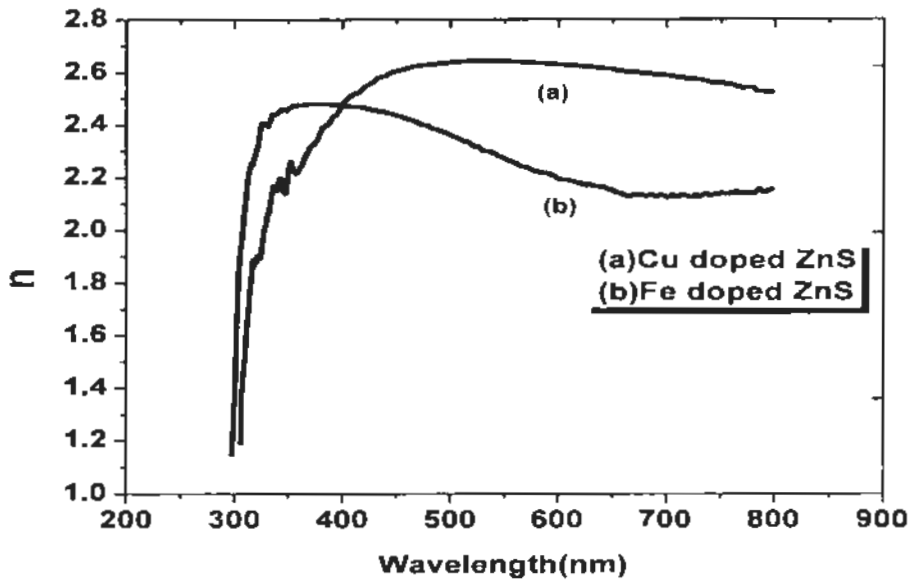


Figure 3.28: Plot of refractive index vs wavelength  $\lambda$  for doped ZnS with Cu and Fe

For all the samples refractive index almost increased with increase in wavelength. Whereas a slightly decreased behavior is observed with Fe doped samples of ZnS films in the visible range. For Cu doped film, refractive index increases till 450nm and for  $\lambda$  larger than 450nm it almost remained constant. Because of the changing refractive index in spectrum, visible wavelength can be separated. The reason for this behavior is that each wavelength will be deviated by different angles. This is reflecting strong dispersion properties of these films.

### 3.4.7 Extinction coefficient, k

This is the measure of absorption when the radiation travels a distance in the sample equal to its wavelength in free space. It is also related to absorption coefficient  $\alpha$  by [40, 42]

$$K = \frac{\alpha\lambda}{4\pi} \dots \dots \dots (3.8)$$

Values of K for different films are calculated from  $\alpha$  and are plotted in fig.3.29-3.31.

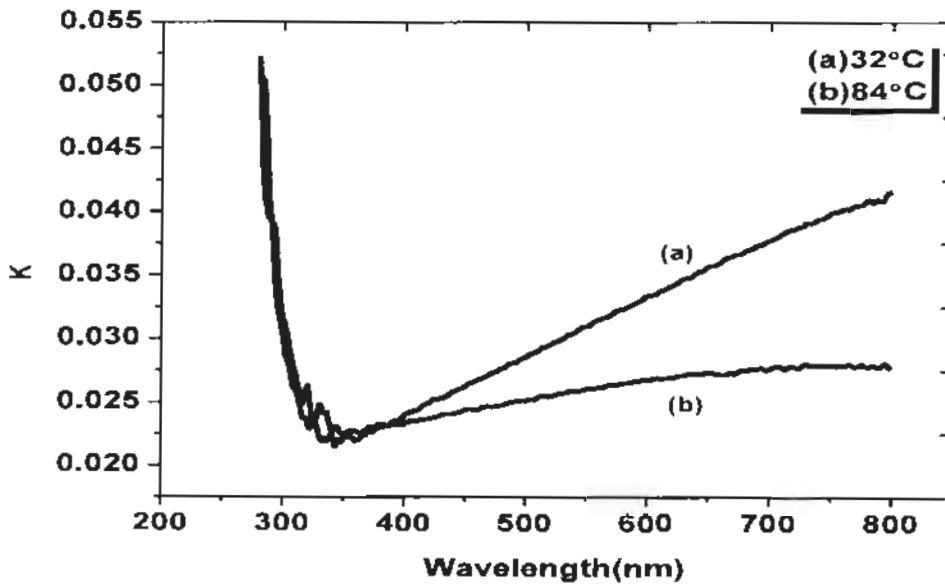


Figure 3.29:: Extinction coefficient graph of ZnS thin films deposited at different temperature (3hrs)

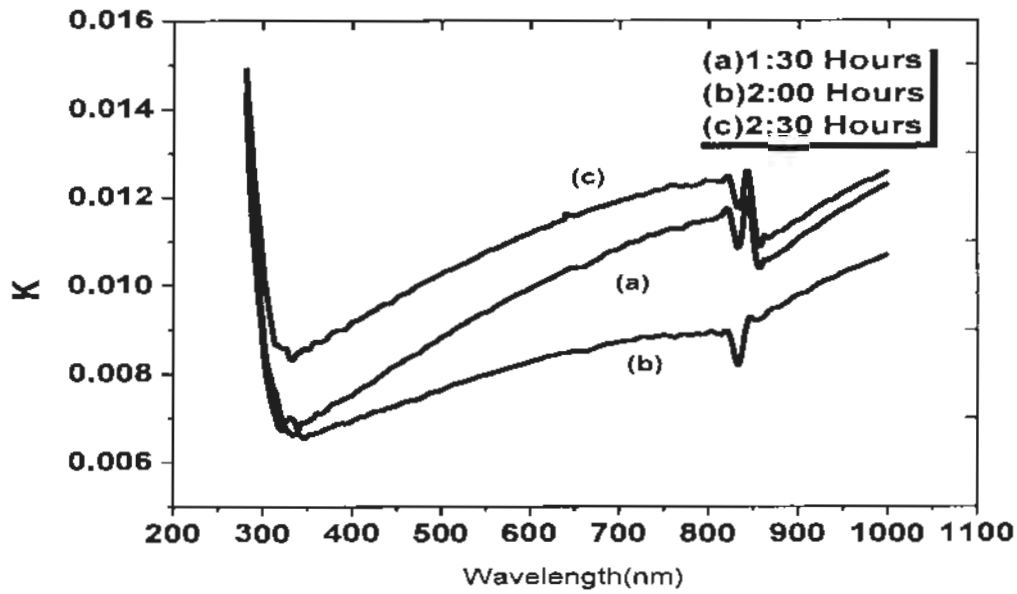


Figure 3.30: Extinction coefficient graph of ZnS thin films deposited at different deposition time (84°C)

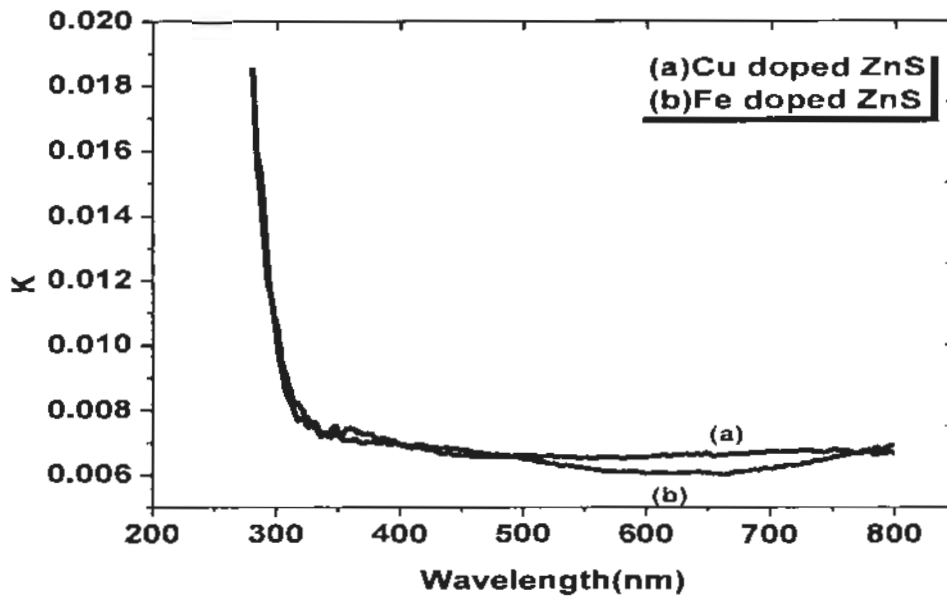


Figure 3.31: Extinction coefficient graph for doped ZnS with Cu and Fe

Extinction coefficient first decreases then increases in all ZnS samples. Whereas in case of doping its value decrease and then remains constant. In the case of a material with direct band gap such as ZnS the minimum energy of the conduction band and the maximum energy of the valance band occur at the same k-value, and in order to excite an electron across the forbidden band a photon of energy  $E_g$  is sufficient. So the materials with high or increasing extinction coefficient probably absorb photons more readily, which are important for excitation of electrons. Thus ZnS can be used in solar cell design.

### 3.4.8 Real dielectric constant

Real dielectric constant can be expressed as the ratio of charge on the plates with free space between the plates ( $Q_0$ ) to charge on the plates with a dielectric medium( $Q$ ). This can be find by the following equation [41]

$$\epsilon_1 = n^2 - k^2 \dots \dots \dots (3.9)$$

Dielectric constants basically describe the behavior of a dielectric to an applied electric field of any frequency.

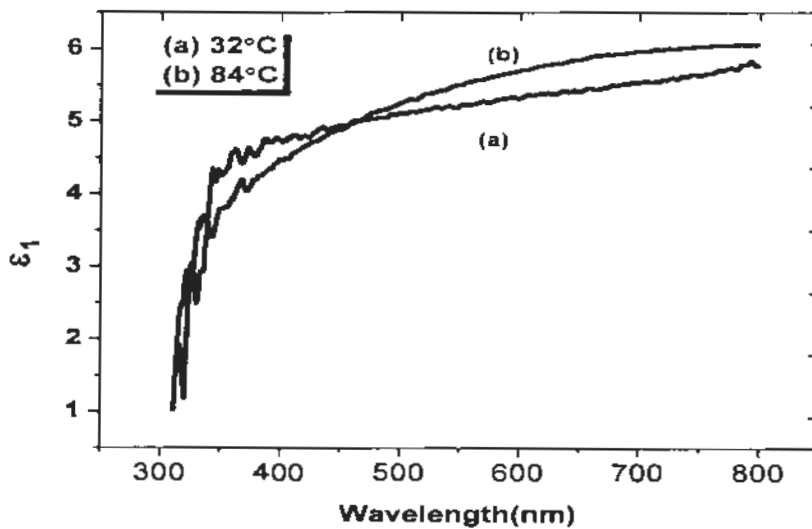


Figure 3.32: Real dielectric constant graph of ZnS thin films deposited at different temperature (3 hrs.)

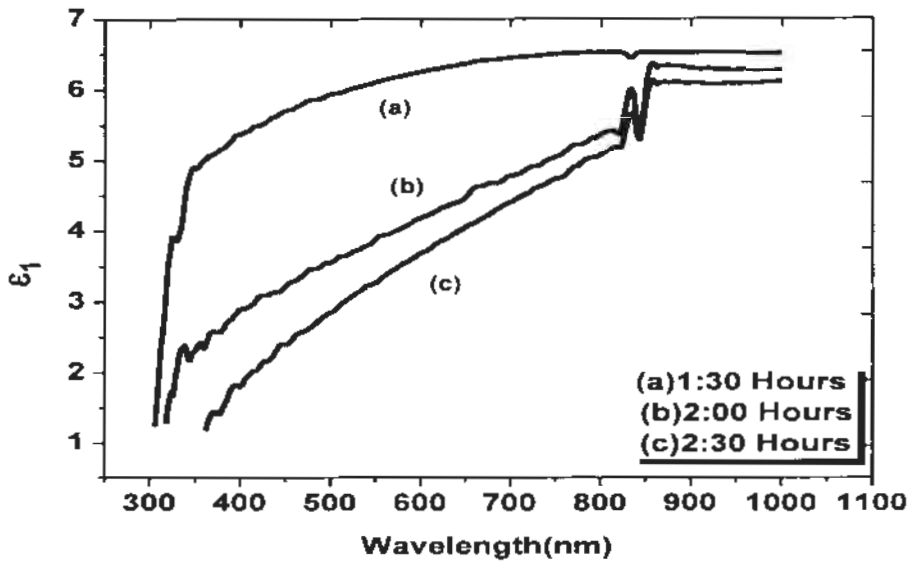


Figure 3.33: Real dielectric constant graph of ZnS thin films deposited at different time (84°C)

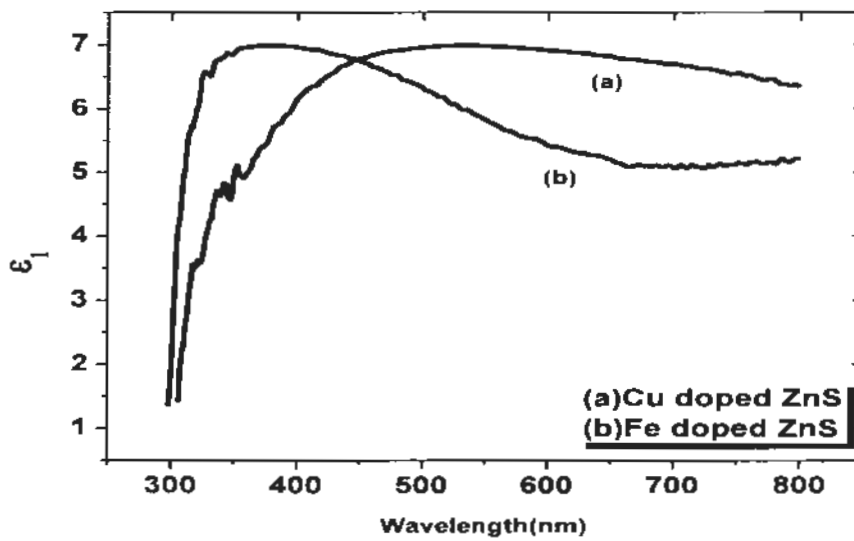


Figure 3.34: Real dielectric constant graph for doped ZnS with Cu and Fe

Figures 3.32-3.34 are related with the graphs of real dielectric constant for all of our samples. These figures shows that in all samples real dielectric constant almost increased with increasing wavelength. Thus thin film samples with high dielectric constant can be used in semiconductors manufacturing process.

### 3.4.9 Imaginary dielectric constant $\epsilon_2$

In order to find imaginary dielectric constant we used the equation as [41]

$$\epsilon_2 = 2nk \dots \dots \dots (3.10)$$

Real dielectric constant can be expressed as the ratio of  $Q_0$  (charge on the plates with free space between the plates) to  $Q$  (charge on the plates with a dielectric medium). During this some of the charges will be out of phase with the applied field, lead to energy loss. A measure of that is imaginary part of dielectric constant. Imaginary dielectric constant for our samples is as shown in fig.3.35 to fig.3.37.

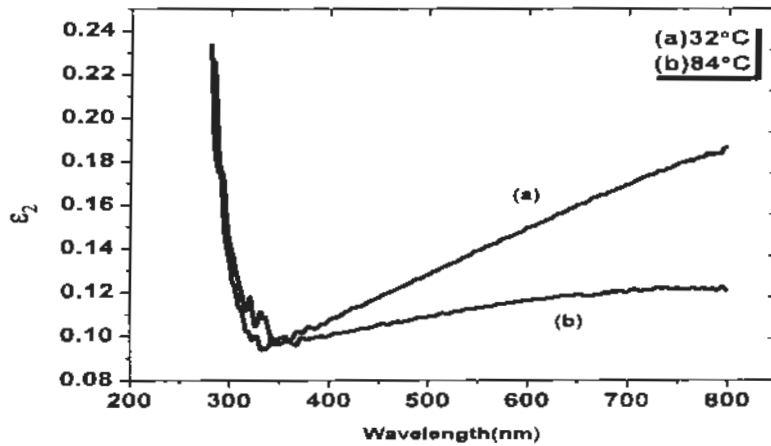


Figure 3.35: Imaginary dielectric constant graph of ZnS thin films at different temperature (3 hrs.)

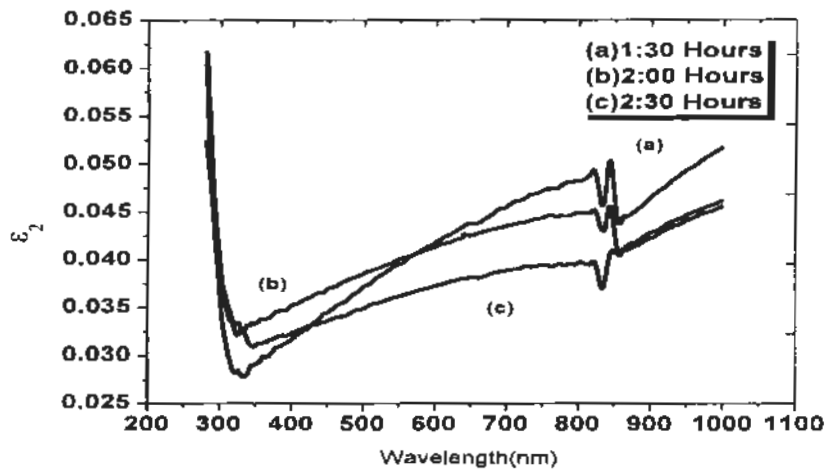


Figure 3.36: Imaginary dielectric constant graph of ZnS thin films deposited at different deposition time ( $84^{\circ}\text{C}$ )



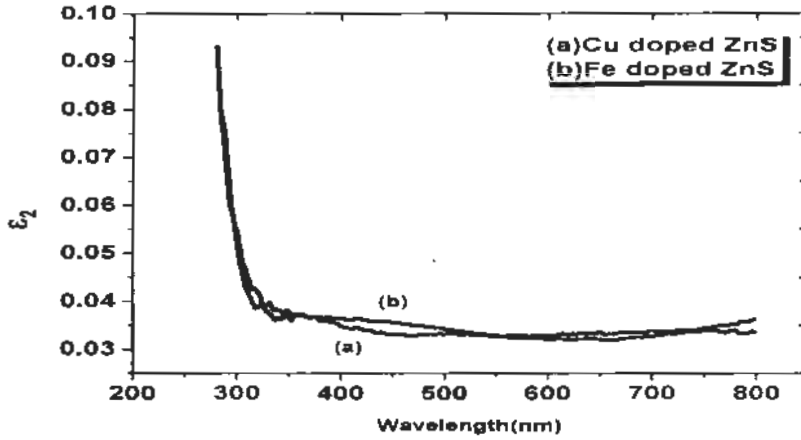


Figure 3.37: Imaginary dielectric constant graph for doped ZnS with Cu and Fe

Figures 3.35-3.37 shows graph for imaginary dielectric constant, calculated by using the equation 3.10. In all these figures we observed that our prepared samples shows almost a decreasing behavior for imaginary dielectric. This decreasing behavior of imaginary dielectric constant is good in the manufacturing process because when losses of charges are minimum in a product, than we can obtain excellent products in semiconductor industry.

### 3.4.10 Optical conductivity

The number of photons absorbed per second by the film is optical conductivity. In designing a solar cell optical conductivity is an important parameter. It is related with absorption coefficient by following relation [41]

$$\sigma = \frac{\alpha n c}{4\pi} \dots\dots\dots(3.11)$$

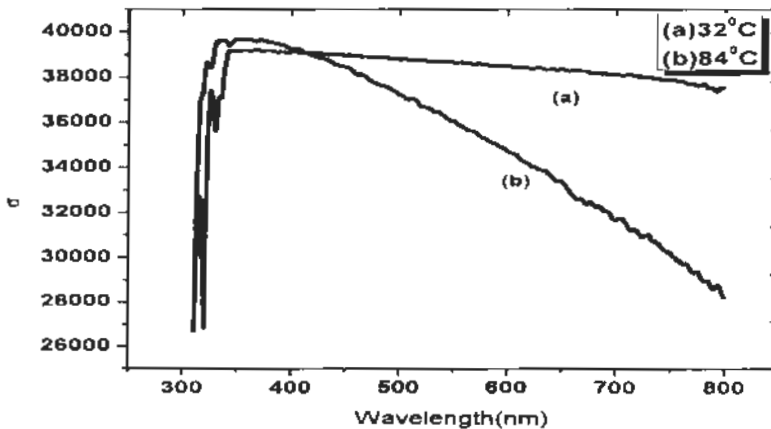


Figure 3.38: Optical conductivity graph for ZnS thin films at different temperature (3 hrs.)

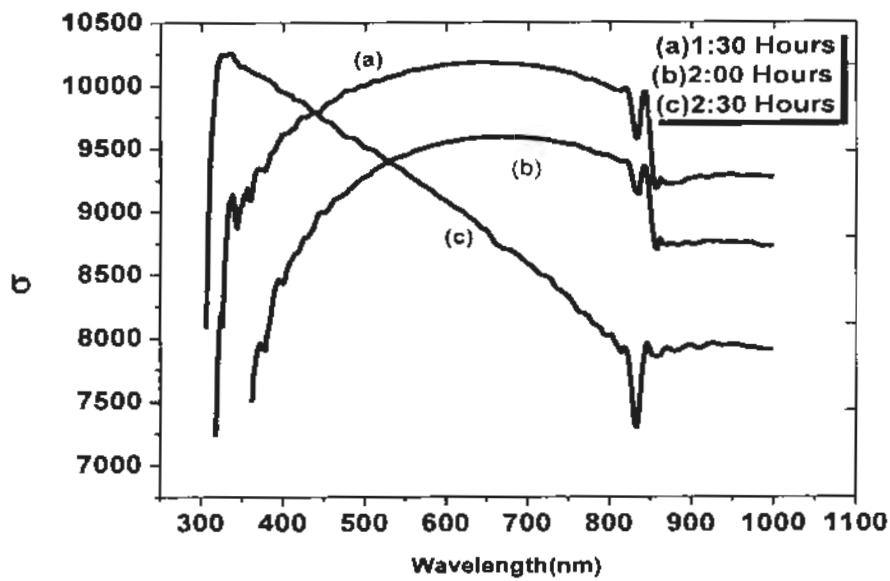


Figure 3.39: Optical conductivity graph for ZnS thin films deposited at different deposition time (84°C)

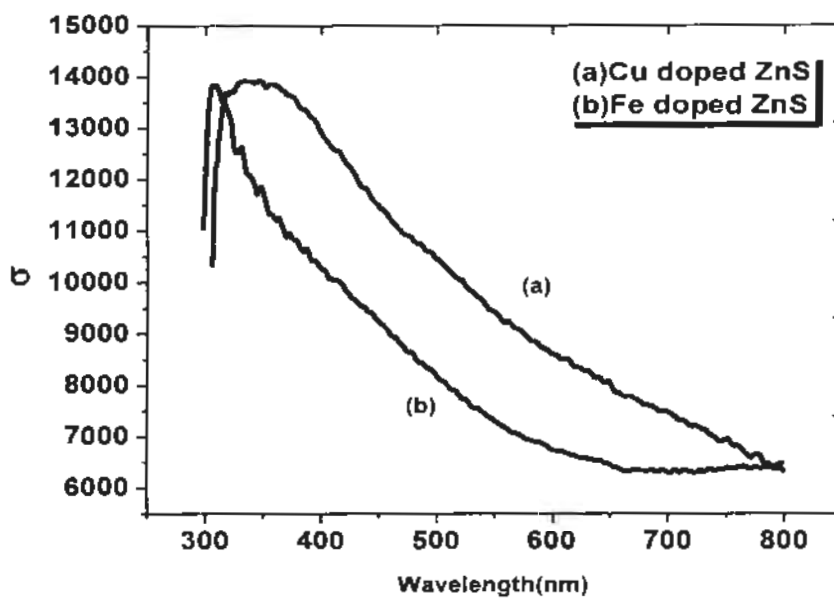


Figure 3.40: Optical conductivity of ZnS doped with Cu and Fe

Optical conductivity variation with wavelength is shown in figures 3.38-3.40. From figures, we observe that  $\sigma$  in all samples shows two different aspects. From the data obtained through UV-Vis spectroscopy,  $\sigma$  increases in UV range and decreases as we move from UV to visible range. There is a gradually decrease in ZnS thin film deposited at different temperatures and in the case of doping, whereas in case of different deposition time this gradually decreasing behavior is not observed. Thus overall in all samples the highest value of optical conductivity is achieved in UV region, so prepared ZnS films can also be used as UV absorber.

### 3.5 Ellipsometry

We also determine optical properties of the thin films deposited on glass substrate are determined by using ellipsometry and then compared them with those obtained from UV Vis spectroscopy. Details of the measurements and then step by step analysis are given in coming section.

#### 3.5.1 Refractive index

Refractive index was recorded through ellipsometry as shown in figure 3.41-3.43. In all these figures we observed an increasing trend of refractive index for all samples of doped and undoped ZnS thin films using chemical bath deposition method.

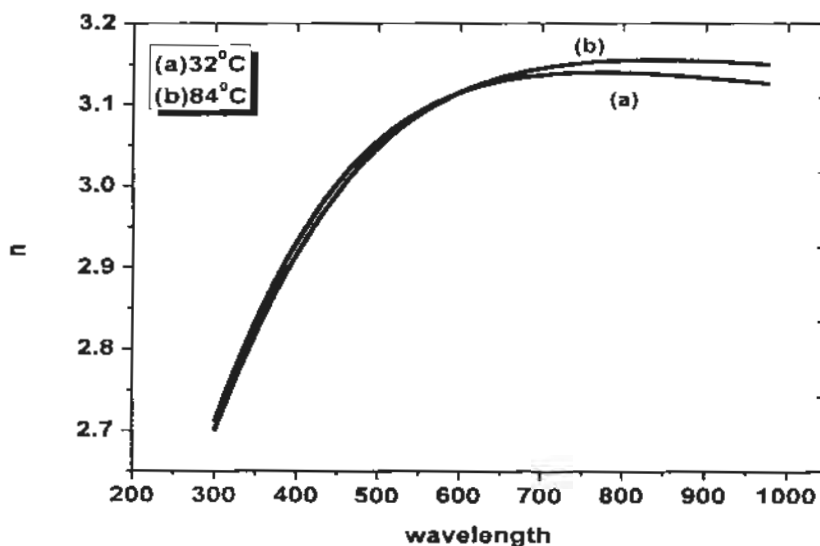
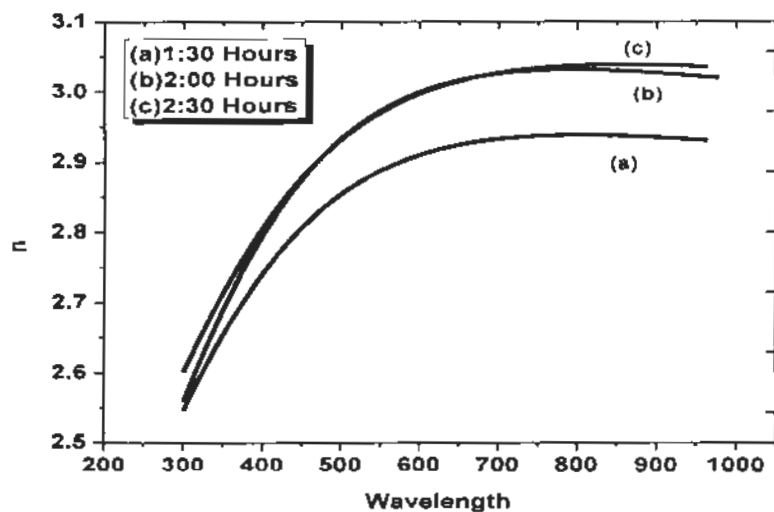


Figure 3.41: Plot of refractive index vs wavelength  $\lambda$  of ZnS thin films deposited at different temperature (3hr) from ellipsometry



Figures 3.42: Plot of refractive index vs wavelength  $\lambda$  of ZnS thin films deposited at different deposition time ( $84^{\circ}\text{C}$ ) from ellipsometry

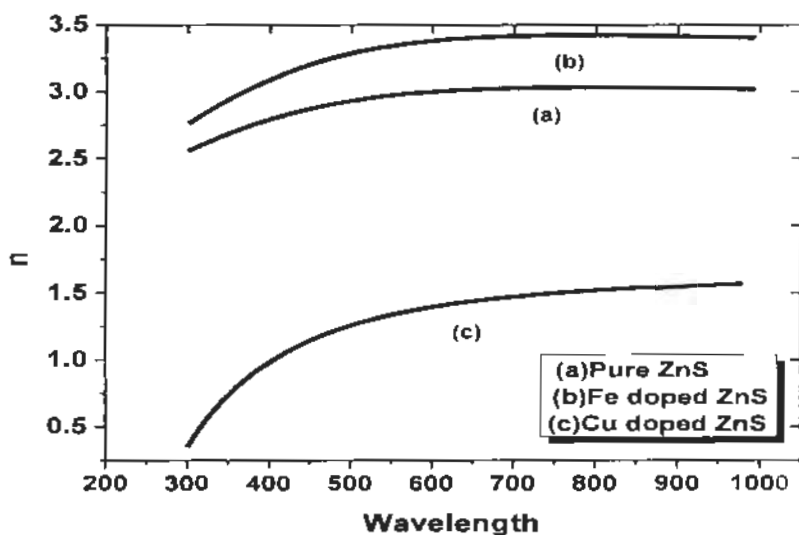


Figure 3.43: Plot of refractive index vs wavelength  $\lambda$  for undoped and doped ZnS with Cu and Fe from ellipsometry

From comparison of these figures with figures 3.26-3.28 it was observed that, although there is difference in refractive index values obtained from UV-Vis spectrum and ellipsometry but the increasing trend of refractive index remains the same. This difference is due to the fact that, refractive index of glass substrate is also incorporated in ellipsometry. In figure 3.43, it can be

seen that pure ZnS film has a refractive index value, intermediate between doped samples of ZnS with Cu and Fe. This is due to the increased stress in films by doping of metals in ZnS.

### 3.5.2 Extinction coefficient

From ellipsometry we obtained the extinction coefficient as shown in figures 3.44-3.46.

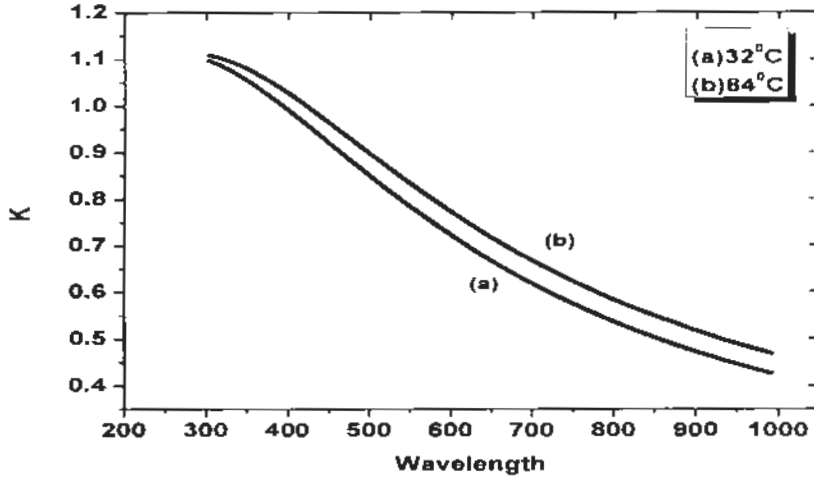


Figure 3.44: Extinction coefficient graph of ZnS deposited at different temperatures (3 hrs) from ellipsometry

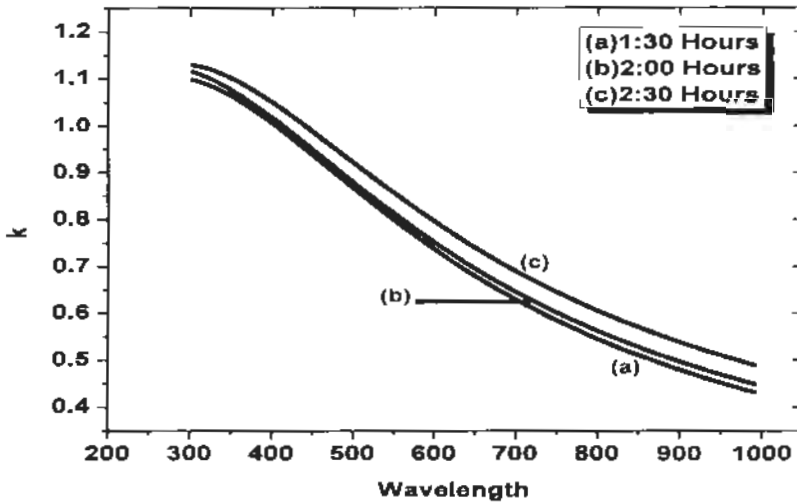


Figure 3.45: Extinction coefficient graph of ZnS deposited at different deposition time (84°C) from ellipsometry

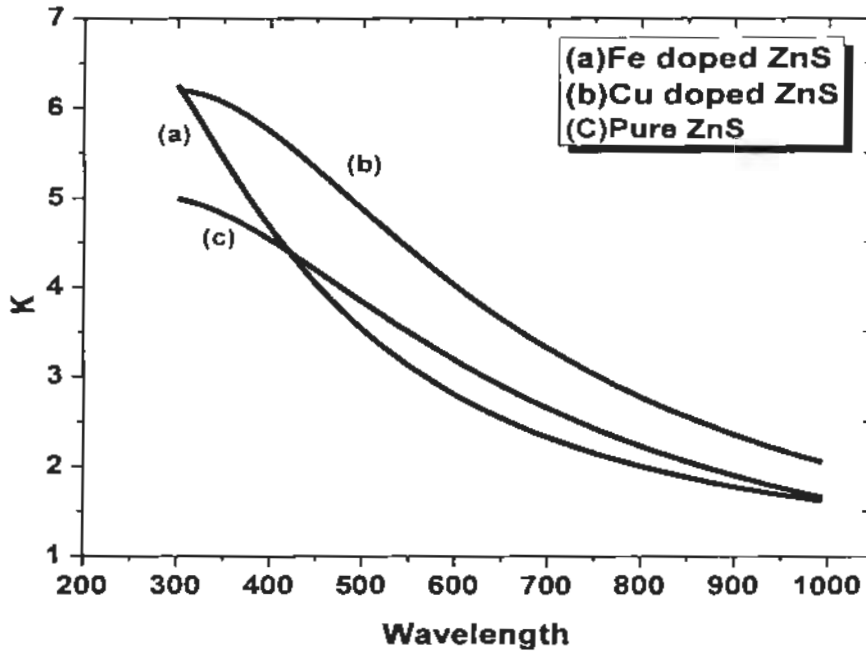
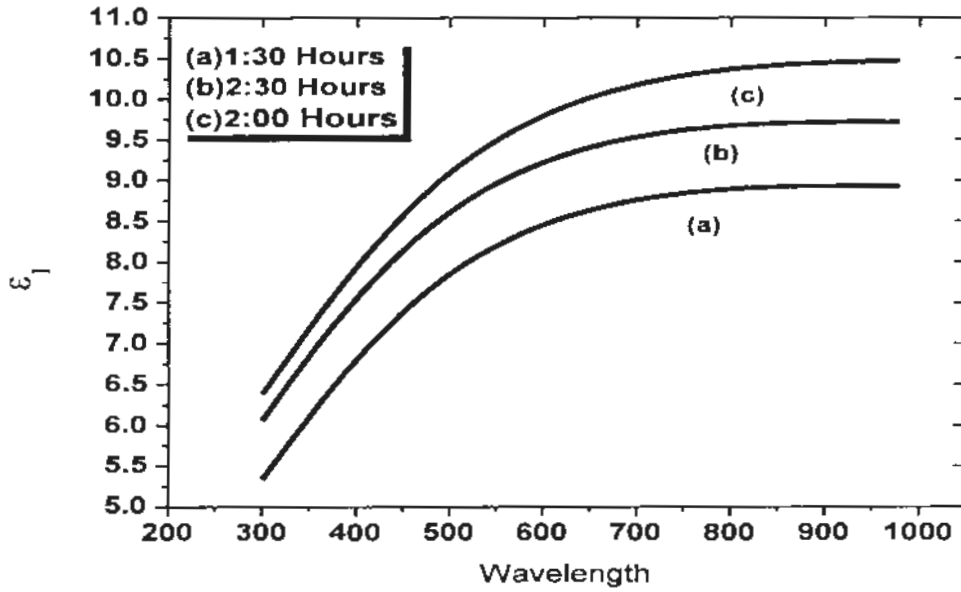


Figure 3.46: Extinction coefficient graph of undoped and doped ZnS with Cu and Fe from ellipsometry

These figures show a decreasing trend for extinction coefficient as the wavelength is increased. By comparing results for  $K$  obtained through ellipsometry and UV-Vis transmission spectroscopy, it is clear that variation with wavelength is different in two cases. For the data obtained through UV-Vis spectroscopy,  $K$  decreases rapidly and increases as we move from UV to visible range. The trend is different as the two techniques are measuring slight different response. UV-Vis spectroscopy measures direct transmission incorporating the effect of substrate whereas in the case of ellipsometry we try to rule out effect of substrate through proper models.

### 3.5.3 Real dielectric constant

Real dielectric constant was recorded through ellipsometry as shown in figures 3.47-3.49.



Figures 3.47: Real dielectric constant graph of ZnS at different deposition time (84°C) from ellipsometry

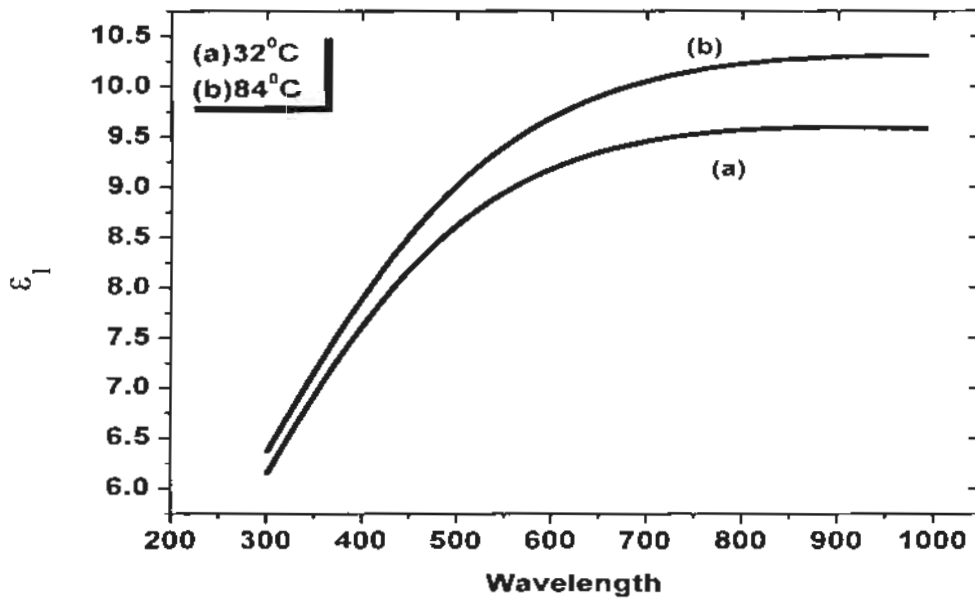
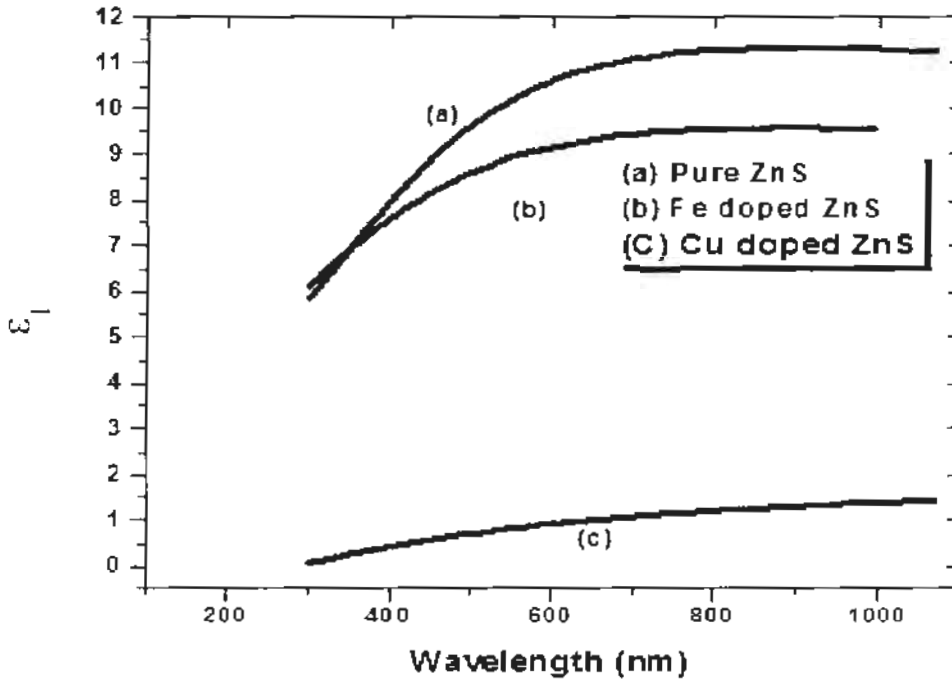


Figure 3.48: Real dielectric constant graph of ZnS deposited at different temperature (3 Hrs.) from ellipsometry



Figures 3.49: Real dielectric constant graph of undoped and doped ZnS with Cu and Fe from ellipsometry

Figures shows real dielectric constant of all our samples that was obtained through ellipsometry. In all figures value of real dielectric constant  $\epsilon_1$  is increasing and this increasing trend match well with our UV-Vis transmission results. Thus thin film samples with high dielectric constant can be used in semiconductors manufacturing process.

### 3.5.4 Imaginary dielectric constant

From ellipsometry we also obtained imaginary dielectric constant  $\epsilon_2$ , which are as shown in figures 3.50-3.52. We can observe decreasing trend of imaginary dielectric with wavelength  $\lambda$ , which is accordance with our UV-Vis spectrum. This behaviour is good, for the manufacturing process in semiconductor industry. From comparative study with figures 3.35-3.37, dielectric constant  $\epsilon_2$  decreases rapidly and then increases as we move from UV to visible range. This different trend arises due to two reasons. One main reason is the stresses in the films because of thermal expansion and non-uniform layer of films on glass substrate. Second reason is that, UV-Vis spectroscopy measures direct transmission incorporating the effect of substrate where in ellipsometry, we try to rule out effect of substrate through proper model.



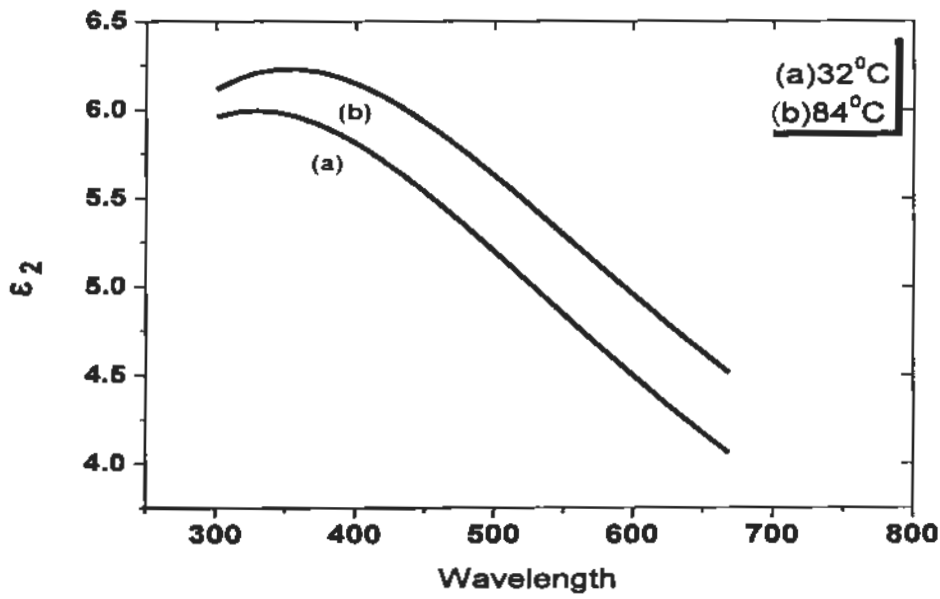


Figure 3.50: Imaginary dielectric constant graph of ZnS deposited at different temperatures (3 Hrs.) from ellipsometry

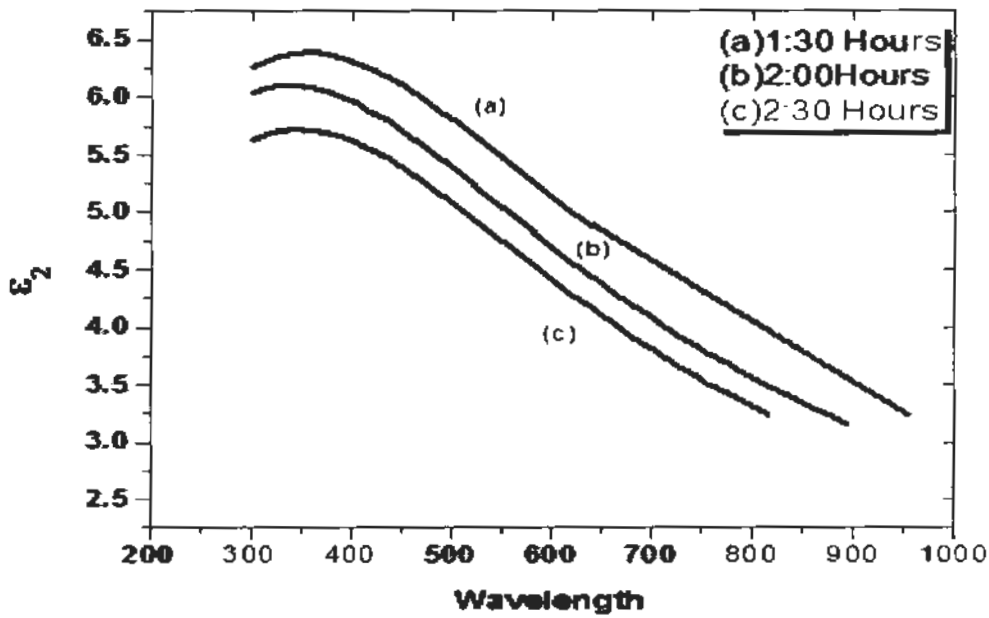


Figure 3.51: Imaginary dielectric constant graph of ZnS at different deposition time (84°C) from ellipsometry

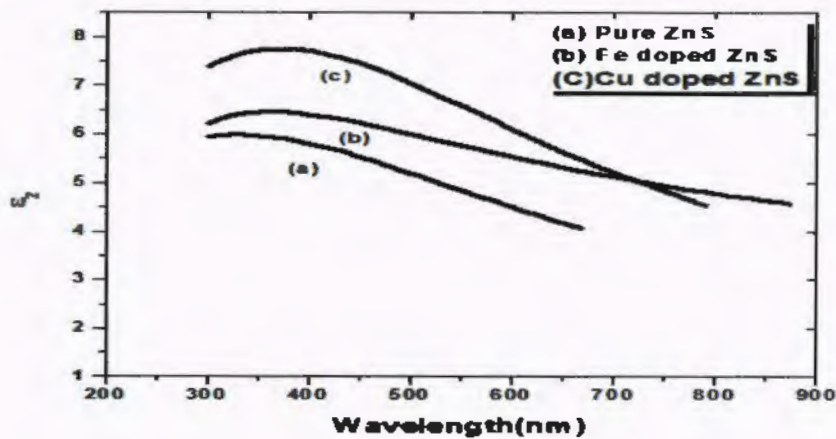


Figure 3.52: Imaginary dielectric constant graph of undoped and doped ZnS with Cu and Fe from ellipsometry

### 3.5.5 Band gap

From ellipsometry data, we also calculated the band gap for all our samples by using tauc equation (3.7). Following table contains the bandgap of ZnS films deposited at different temperature

Table 3.9: Comparison of Band gap values of ZnS films from ellipsometry & UV-Vis spectroscopy

Samples	Band gap from ellipsometry	Bandgap from UV-Vis spectroscopy
ZnS at 32°C (3 Hours)	3.06	3.75
ZnS at 84°C (3 Hours)	3.08	3.6

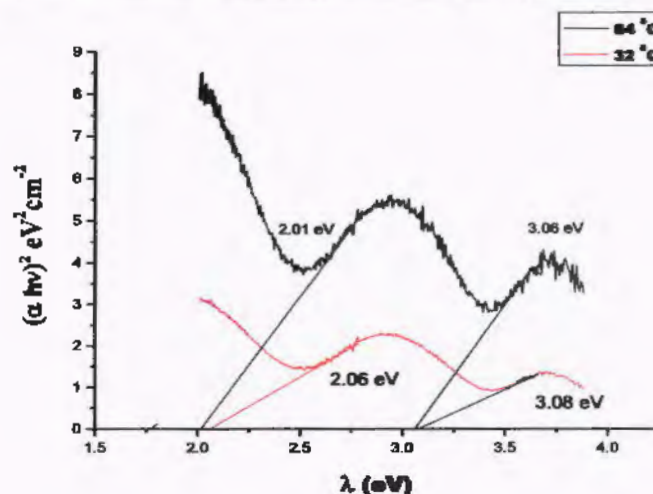
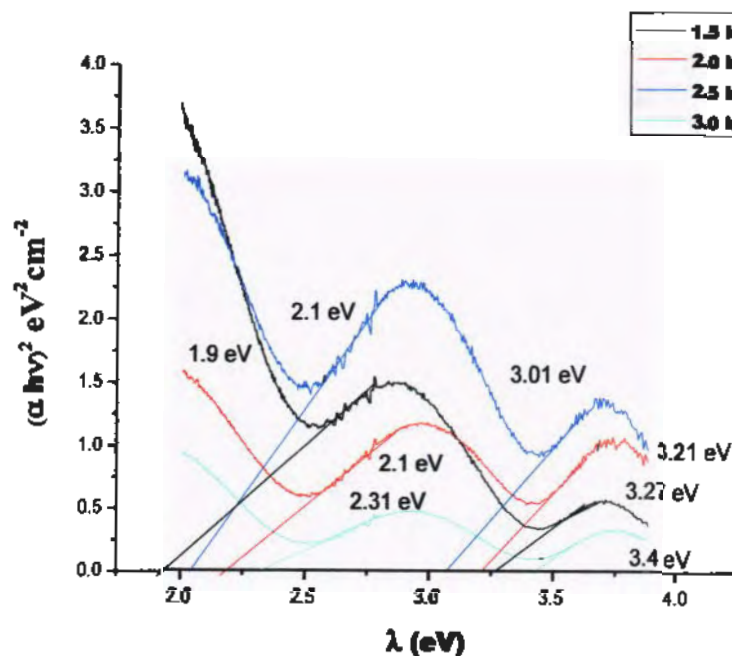


Figure 3.53: Band gap values of ZnS films deposited at different temperature (3 hrs) from ellipsometry

From these calculated values we observed that band gap of our prepared ZnS film decrease with the increase in temperature, which is consistent with the band gap obtained from UV Vis spectroscopy data. This decrease in band gap is favorable in designing solar cell. On the other hand, an additional band gap was also observed in graph, which was attributed to the conduction band tail states arising from the impurity, doping or due to the formation of both wurzite and sphalerite structures of ZnS that extends the conduction band. Sajid Ali et al. also achieved similar pattern of dual band gap [45, 46]. Similarly in second case we prepared the samples at same deposition temperature, but different deposition time. Band gap of these samples are as

*Table 3.10: Comparison of Band gap values of ZnS films from ellipsometry & UV-Vis spectroscopy*

Samples	Band gap eV from ellipsometry	Band gap eV from UV-Vis spectroscopy
ZnS at 84°C (1:30 Hours)	3.0	3.9
ZnS at 84°C (2:00 Hours)	3.21	3.75
ZnS at 84°C (2:30 Hours)	3.27	3.62
ZnS at 84°C (3:00 Hours)	3.4	3.60



*Figure 3.54: Band gap values of ZnS films deposited at different deposition time (84°C) from ellipsometry*

When we change the deposition time we observed that band gap of our samples increased with increasing in deposition time. This specific behavior of band gap is due to more deposition time given to ZnS nuclei to settle down on substrate. This behavior is also desirable for many applications. Now in case of doped samples band gap values are shown in table 3.11.

*Table 3.11: Comparison of Band gap values of doped ZnS films from ellipsometry & UV-Vis spectroscopy*

Samples	Band gap eV from ellipsometry	Bang gap eV from UV-Vis spectroscopy
ZnS	3.4	3.60
Fe doped ZnS	3.1	3.9
Cu doped ZnS	3.3	3.7

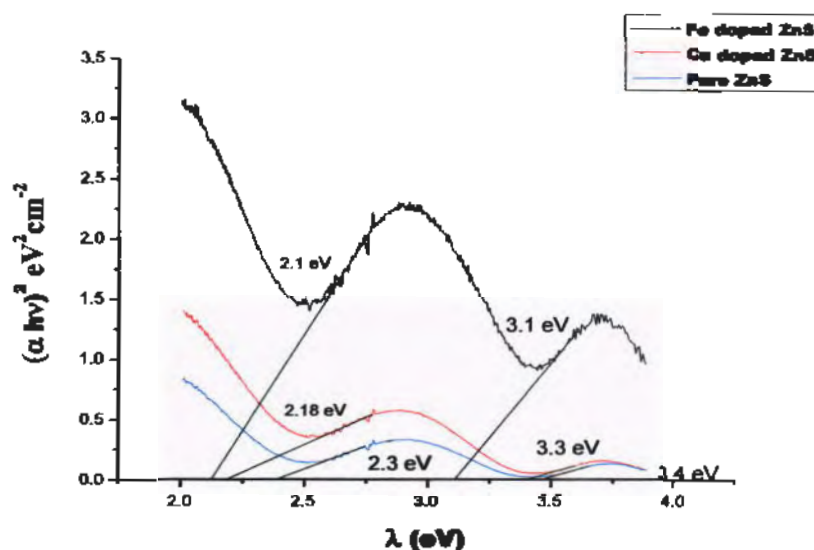


*Figure 3.55: Band gap values of undoped and doped ZnS with Cu and Fe from ellipsometry*

ZnS films doped with Cu and Fe showed decreased band gap of 3.3 eV and 3.1 eV respectively. These ellipsometry results are different to the band gap obtained by UV-Vis spectroscopy. The difference in graph patterns is due to the difference in wavelength range of both of the instruments. Moreover, general equations, irrespective of the samples, are used to analyze UV-Vis data whereas special models, based on the type of samples, are used in ellipsometry. These factors resulted in faintly altered band gap values calculated by ellipsometry while the increase in band gap induced by doping is confirmed as directed by UV-Vis spectroscopy.

### 3.6 Conclusions

ZnS thin films were prepared by CBD on glass substrate. Certain reaction parameters such as temperatures and deposition time were varied and corresponding effects on prepared films were observed. Doped samples of ZnS with Cu and Fe on glass substrate were also prepared by CBD.

The thickness of films is 26-30 nm. In case of different deposition time, films were covered with larger particles. The particles were sparsely arranged and the average particle size increased with the increase of deposition time. This indicated that longer deposition time would mainly affect the growth of particle with the same deposition temperature. Similarly the grain size increases and the film surface becomes more uniform the increase in the deposition temperature. This indicates that a higher deposition temperature will mainly affect the homogeneous process for the ZnS thin film deposited at the same time. XRD patterns showed that all the undoped and doped ZnS films were amorphous whereas XRD pattern of ZnS films in case of doping induced more amorphous nature as compared with undoped samples. The band gap of synthesized films was determined by UV-VIS spectroscopy and ellipsometry. The calculated ZnS band gap values were in the range of 3.6-3.9 eV, while doping increased the band gap of synthesized films up to the values 3.89 eV (Cu doped ZnS) and 3.90 eV (Fe doped ZnS). Electrical responses of the samples were more or less resistive. SEM images showed an increase in granular structure with the increase in temperature and deposition time. Furthermore, the addition of Cu and Fe in the ZnS films also induced modifications to morphology of the films by showing elongated aggregates or rod like structures instead of spherical ones of undoped ZnS films.

### 3.7 Future Prospects

Synthesized ZnS thin films can be utilized in various applications such as solar cells, as a catalyst and in opto-electronics devices. The properties of the films can be modified by changing the substrate, dopants and certain reaction parameters like precursors, solution pH, deposition time and deposition temperature. Properties of these films may also be varied by changing the amount of dopants, deposition temperature and dopants. In future we will also observe the corresponding changing in properties of films by changing the amount of dopants respectively.

## References

1. Chopra, K.N., Scientist G(Retd)Laser Science &Technology centre Metcalfe House Delhi-110 054.
2. Seshan, K., "*Handbook of Thin Films Deposition processes & Techniques, Principles, Methods, Equipment and Applications, 2nd Edition*". NOYES PUBLICATIONS.
3. D.S. Dhawale, A.M.M., S.S. Lathe, K.Y. Rajpure, C.D. Lokhande, Applied Surface Science, 2008. **254**: p. 3269-3273.
4. P.Jackson, D.H., S. Paetel, Photovoltaics, 2011. **19**: p. 849-897.
5. M.A. Contreras, T.N., M. Hongo, A.O. Pudov, J.R Sites, in:Proceedings of the 3rd World Conference on Photovoltaic Energy Conversion, Osaka, Japan, 2003: p. 570-573.
6. D.V. Petrov, B.S.S., G.A.L. Pereira, C.D.M. Donega, phys, Chem. B, 2002(5325): p. 106.
7. WWW.WIKIPEDIA.COM.
8. WWW.reade.com.
9. I.O. Oladeji, L.C., Thin Solid Films, 2005. **474**: p. 77-83.
10. M. Zafar Iqbal, *A text book of organic chemistry*. Punjab book board pakistan, 2009.
11. B. Egon Wildermuth, H.S., Gabriele Friedrich, Franz Ludwig Ebenhöch, Brigitte Kühborth, Jack Silver, Rafael Rituper "Iron Compounds" in Ullmann's Encyclopedia of Industrial Chemistry Wiley-VCH, Wienheim, 2005.
12. I.O. Oladeji, L.C., J.R. Liu, Thin Solid Films 359 (2000) 154.
13. F. Go` de, C.G.m.s., M. Zor, J. Cryst. Growth 299 (2007) 136.
14. O.L. Arenas, M.T.S.N., P.K. Nair, Semicond. Sci. Technol. 12 (1997) 1323.
15. T. Negami, T.A., T. Satoh, Proceeding of the 29th IEEE, PVSC, New Orleans, and p. 2002.
16. M.A. Contreras, T.N., M. Hongo, Proceeding of the 3rd World Conference of and Photovoltaic Energy Conversion, p. 242.
17. S. Siebentritt, Sol. Energy, 2004. **77**: p. 767.
18. U. Gangopadhyay, K.K., D. Mangalaraj, J. Yi, Appl. Surf. Sci. 230 (2004) 364.
19. J.M. Don` a, J.H., Thin Solid Films 268 (1995) 5.
20. D.A. Johnston, M.H.C., K.T.R. Reddy, I. Forbes, R.W. Miles, Thin Solid Films and 102.

21. C. Gu"mu" s, C.U., R. Esen, O.M. O" zkendir, Y. Ufuktepe, *Thin Solid Films* 492 and 1.
22. P. Roy, J.R.O., S.K. Srivastava, *Thin Solid Films* 515 (2006) 1912-1917.
23. M. Lodar, E.J.P., I. Baldea, R. Grecu, E. Indrea, *J. Alloys Compd.* 434-435 (2007) 697-700.
24. C. Hubert, N.N., B. Canava, A. Etcheberry, D. Lincot, *Thin Solid Films* 515 (2007) 136-141.
25. J. Vidal, O.V., O. De Melo, N. Lopez, O. Zelaya-Angel, *Mater, Chem. phys.* 61 (1999) 139-142.
26. Cao, G., *NANOSTRUCTURES & NANOMATERIALS*. 2004.
27. Charels P.Poole, J.F., J.Owens, *Introduction to Nanotechnology*. 2003.
28. Fujiwara, H. and J.W. Sons, *Spectroscopic Ellipsometry: Principles and Applications*. 2007.
29. Harland Tompkins, E.A.H. and W. Andrew, *Handbook of Ellipsometry* 2005.
30. Taisuke Iwashita , S.A., *Thin Solid Films*, 2012. **7076-7082** p. 520.
31. Hankare PP, C.P., Sathe DJ, Chavan PA, Bhuse VM. *J Mater Sci Mater Electron* 2009;20:374-9.
32. Qi Liu , M.G., Ao jianping, *Applied Surface Science*, 2008. **254**: p. 5711-5714.
33. Limei Zhou , N.T., Sumei Wu, Xiaofei Hu, Yuzhi Xue, *Physics Procedia*, 2011. **22**: p. 354-359.
34. S. Muthukumaran n, M.A., *Materials Letters*, 2013. **93**: p. 223-225.
35. Muhammad Saeed Akhtar, M.A.M., Yousef G. Alghamdi, Khuram shahzad Ahmed, Saira Raiz, Shahzad Naseem, 2015. **39**: p. 283-291.
36. Wei Y, H.D., Qiao S, Zhen C, Tang G. *Physica B* 2009;4(4):2486-8.
37. Limei Zhou , N.T., Sumei Wu, *Surface & Coatings Technology*, 2013. **228**: p. S146-S149.
38. Limei Zhou, N.T., Sumei Wu, Xiaofei Hu, Yuzhi Xue, *Physics Procedia*, 2011. **22**: p. 354-359.
39. Daniela E.Ortíz-Ramos a, L.G.a., n, RafaelRamirez-Bon, *Materials Letters*, 2014. **124**: p. 267-270.
40. Onwuemeka, J.I., Nwofor, Okechukwu k ., Nwulu, Nobert, Ezike, Fabian M. , Iwuiaia, Chalse C., Olissaeba, Okechukwu, 2013. **2**(11).
41. suresh, S., *American Chemical Science Journal*, 2013. **3**: p. 325-337.

42. Pawan kumar, A.K., P N Dixit & T P Sharma, *Optical, structural, and electrical properties of zinc sulphide vacuum evaporated thin films*. Indian Journal Of Pure & Applied Physics, 2006. **44**: p. 690-693.
43. Swanepoel, R., "*Determination of the thickness and optical constants of amorphous silicon*". J. Phps. E:Sci, 1983. **16**.
44. H.T. Grahn, Lt.S.P., World Scientific Publishing, Singapore, 1999., .
45. Sajid Ali Ansari, M.H.C., nature, 2016.
46. H. B. Russell, A.N.A., M. Menon, J. B. Jasinski, A. Martinez-Garcia & M. K. Sunkara, nature, 2016.

